POLITECNICO DI MILANO

Facoltà di Ingegneria dei Processi Industriali

Dipartimento di
Chimica, Materiali e Ingegneria Chimica “Giulio Natta”

Electrochemical etching of Aluminium foils for capacitors

Relatore: Prof. Maurizio Masi

Elaborato di laurea di
Franco LIONETTI
Matricola 617017

Anno Accademico 2007-2008

INDEX

- INTRODUCTION

- Part I – PIT NUCLEATION BEHAVIOUR

- Part II - TUNNEL GROWTH

- Appendix

- References

INTRODUCTION

Capacitors store energy as well as charge. These charges are generally stored on conductive plates, the positively charged plate called the anode and the negatively charged plate called the cathode (Figure 1).

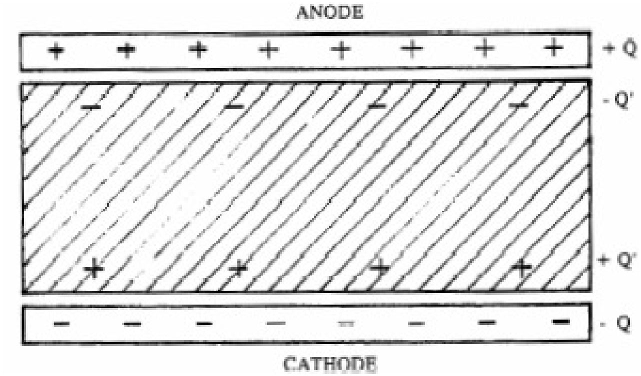

Fig. 1. Charges "Q" on anode and cathode induce charges "Q'" on the dielectric

In order to keep the charges separate, the medium between the anode and cathode, called the dielectric, must be non-conductive – an electrical insulator. The anode and cathode are configured so that very little movement occurs between them as they are charged and the force on the dielectric increases. As the stored charge increases, the electric field across the dielectric increases. This situation gives rise to a voltage which increases proportionally with the charge. The ratio of the charge magnitude on each plate to the electric potential (voltage) between the plates is known as capacitance. The energy stored in a capacitor is the energy required to move the stored charge through the potential of the capacitor. The capacitance of a device depends mostly on the plate geometry and the nature of the dielectric. It is directly proportional to the "dielectric constant" (Table I) and inversely proportional to the thickness of the dielectric.

As the charge and voltage on a given capacitor are increased, at some point the dielectric will no longer be able to insulate the charges from each other. The dielectric then exhibits dielectric breakdown, or high conductivity in some areas, which tends to lower the stored energy and charge, generating internal heat. This phenomenon, undesirable in most capacitor applications, occurs at the capacitor's breakdown voltage. Capacitor damage or destruction can occur in such situations. Normally, breakdown ratings for dielectrics are expressed as a maximum field strength which is basically the ratio of the applied voltage to the dielectric thickness.

The mass energy density of a capacitor is the ratio of the amount of energy the capacitor can store at its working voltage to the capacitor mass, including package. The working voltage of a capacitor is defined as the maximum rated voltage for a given application. The working voltage is generally less than the breakdown voltage. An exception to this rule could occur if the transient peak voltage were able to exceed the steady-state breakdown voltage. The volumetric energy density of a capacitor is defined as the ratio of the energy stored to the capacitor volume, including package.

Dielectric material / Relative dielectric constant "k" (also indicated with “ε” in some literature)

- Air or vacuum / 1.0
- Polypropylene / 2.2
- Polyester (Mylar) / 3.0
- Mica / 6.0
- Aluminum oxide / 8.5
- Tantalum pentoxide / 27
- Niobium oxide / 41
- Barium titanate / 1000 – 10000

Table I. Relative dielectric constants "k" for various dielectrics

The first capacitor was invented in 1745 by Pieter van Musschenbroek, a physicist and mathematician in Leiden, Netherlands (and called the Leyden jar). It was a simple glass jar coated inside and outside with metal foil. William Dubilier invented the mica capacitor in about 1910.

I - Electrolytic capacitors

Electrolytic capacitors are capacitors in which one or both of the "plates" is a non-metallic conductive substance, an electrolyte. Electrolytes have lower conductivity than metals, so are only used in capacitors when metallic plate is not practical, such as when the dielectric surface is fragile or rough in shape or when ionic current is required to maintain the dielectric integrity. The dielectric material of electrolytic capacitors is produced from the anode metal itself in what is known as the forming (or anodizing process). During this process, current flows from the anode metal – which must be a valve metal such as aluminum, niobium, tantalum, titanium, or silicon – through a conductive bath of a special forming electrolyte to the bath cathode. The flow of current causes an insulating metal oxide to grow out of and into the surface of the anode. The thickness, structure and composition of this insulating layer determine its dielectric strength. The applied potential between the anode metal and the bath cathode must be above the oxide breakdown voltage before significant current will flow. As current flows, the breakdown strength (formed voltage) and oxide thickness increase. See Figure 2 for a comparison of the electrostatic (classical) and electrolytic capacitors. The "electrolytic capacitors" are quite different from, and not to be confused with the "electrochemical capacitors" (also called ultracapacitors) the operation of which is based on the electrical double layer capacitance.

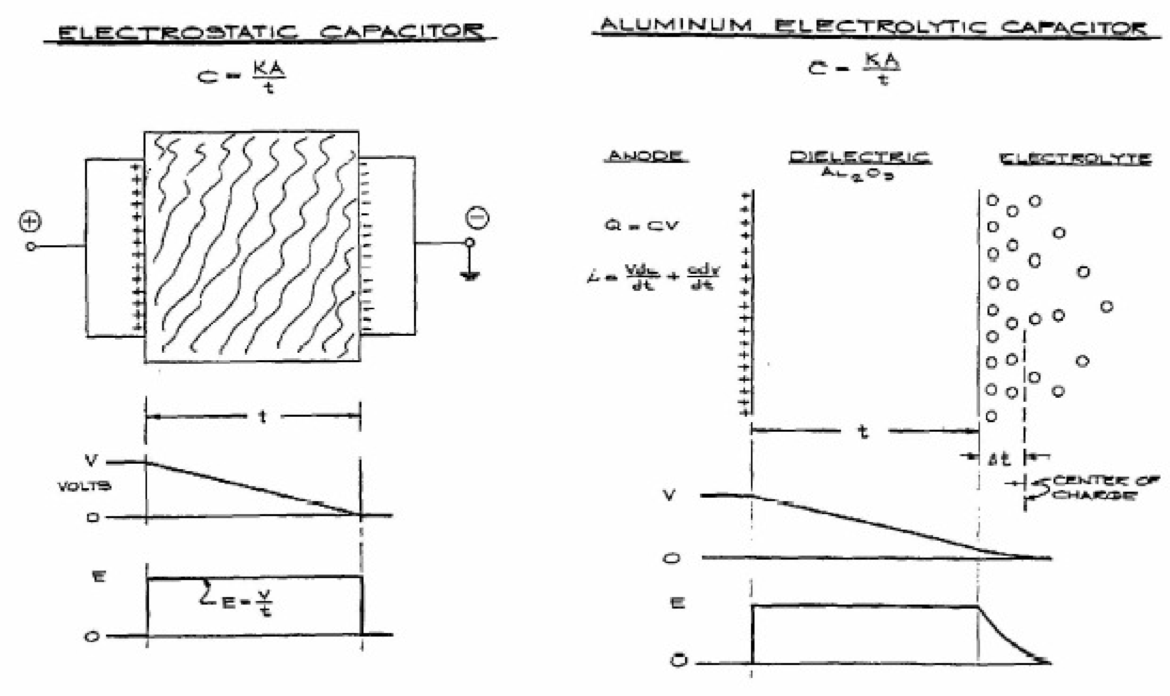

Fig. 2. Comparison of electrostatic and electrolytic capacitors.

The electrolysis reaction was investigated by Michael Faraday in the 1700's. A relationship between the charge flow through the system and the amount of product (in this case, metallic oxide) was found to exist. Faraday noted the relationship between gram-equivalents of product and charge transfer for all ideal (stoichiometric) electrolysis reactions in what is now known as Faraday's Law. Departures from this relationship exist for the process of oxide formation on anode metals, since some oxide can be grown chemically and thermally to reduce the electrical energy requirements in the formation process, which can cost several dollars per kilogram of anode produced. Also there can be some undesirable side reactions during the formation process which do not contribute to oxide formation. In the formation process, brittle metallic oxide is grown upon the metal foil, which is usually rough in shape. The anode metal is therefore in intimate contact with one side of the oxide dielectric. The electrolyte is used to make contact between the other side of the oxide and the cathode plate.

The advantage of electrolytic capacitors is the high capacitance per unit volume and per unit cost. The high capacitance arises from the high dielectric constant, the high breakdown field strength, the rough surface, and the extremely small, uniform thickness of the anodically formed metallic oxide. The reason that electrolytic capacitors have such uniform dielectric stress and can operate at such high field strength, within 80% of their breakdown strength, on the order of 1000 volts/µm, is due to two reasons. First, the original anodization ("formation") process is performed at a fixed voltage, and the dielectric grows everywhere to whatever thickness is required to support that voltage. Second, once the foil is in a capacitor, the capacitor "fill" electrolyte continues the healing work of the original forming electrolyte, repairing and thickening the dielectric locally as required. This healing process is driven by the capacitor's DC leakage current, which is drawn whenever a DC voltage is applied to the capacitor, that is, whenever it is in operation. In fact, electrolytic capacitors often last longer when they are in continuous, mild use that when they are only charged up briefly every year or decade.

The disadvantage of electrolytic capacitors is the non-ideal, lossy characteristics which arise from the semiconductive oxide properties, double-layer effects from the electrolyte-oxide charge-space region, resistive losses from the high electrolyte resistivity, frequency response rolloff due to the roughness of the surface oxide, and finite capacitor life due to breakdown and degradation of the electrolyte. Some of these considerations will be discussed below in more detail from the standpoint of the aluminum electrolytic capacitor.

Also, the anodic oxide dielectric is polar, and so are the electrolytic capacitors (in contrast with the classical, electrostatic capacitors), that is the capacitors must be connected with the correct polarity as marked. Connecting with reverse voltage injects hydrogen ions through the oxide readily, causing high electrical conduction, heating and reduction of the anodic oxide film. Non-polar (or bi-polar) devices can be made by using two anodes instead of an anode and a cathode, or one could connect the positives or negatives of two identical device together, then the other two terminals would form a non-polar device.

Most electrolytic capacitors are constructed using aluminum electrodes, but tantalum and niobium is also used. Aluminum anode is the least expensive at $0.04 per gram. As such, it is used in large (even greater than one liter!) and small (tiny surface-mount) capacitors. Tantalum anode material is over $2.00 per gram but offers high stability, more capacitance (four times that of aluminum), lower resistance (up to 90% lower) per size. It is available as small units (typically less than 5 cm^3) and surface mount. Niobium anodic powder is less than $1.00 per gram, much cheaper and more available than tantalum but still much more expensive than aluminum. Capacitance is much more than aluminum, nearly that of tantalum. It is a much newer technology than tantalum.

H.O. Siegmund invented the electrolytic capacitor in 1921. Julius Lilienfeld did much to develop electrolytic theory in the 1920's and 1930's. Cornell Dubilier was at this time the world's largest capacitor company, and did much to develop the technology of etching and anodizing.

II - Construction details of a wet aluminum electrolytic capacitor

Production process

Aluminum electrolytic capacitors are comprised of anode and cathode plates separated by an absorbent spacer. As shown in Figure 3, metal tabs are attached to the anode and cathode plates, and the assembly is wound into a cylindrical section. The tabs are welded to aluminum terminals installed in a header (top). The section-header assembly is immersed in a bath of hot capacitor electrolyte (significantly different from the formation process electrolyte). In what is called the impregnation process, a vacuum is applied to the electrolyte and sections, causing electrolyte to be drawn into the sections, thoroughly wetting the sections. The sections are placed in aluminum cans, and the headers are sealed to the cans. The capacitor units are slowly brought up to maximum rated voltage at maximum rated temperature during the aging process. The aging process grows oxide on areas on the anode foil which have an insufficient oxide barrier, such as slit edges and places which have been cracked during the winding operation. Inspections and tests occur at several stages of the production process.

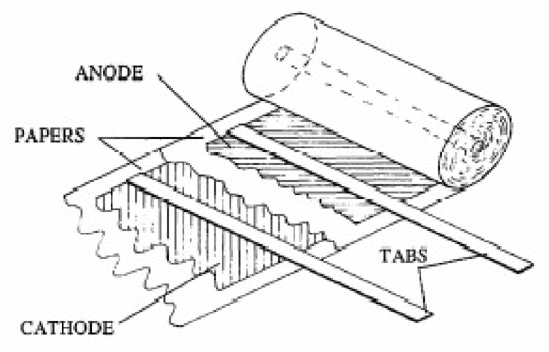

Fig. 3. Construction of an electrolytic capacitor

Anode

The anode can be made of various purities of aluminum, but for high voltage, high energy density aluminum electrolytic capacitors, the anode is generally comprised of 99.99% purity, high cubicity aluminum foil of about 100-micrometer thickness. The term high cubicity refers to the rectangularly oriented aluminum grain structure which is intentionally produced in the foil. The anode foil is generally produced in rolls of 270-kg mass and 48-cm width. The first production process this foil undergoes is called etching, which electrochemically roughens the surface of the foil, causing hollow tunnels to grow into the aluminum. The rectangular aluminum grain orientation causes the etched tunnels to form along parallel paths which are mostly perpendicular to the aluminum top surface. The etching process greatly increases the microscopic to macroscopic surface area ratio, called the "foil gain", which can be up to sixty for high-voltage aluminum electrolytic anode foil, and even higher for low-voltage foil. The foil emerges from the etching process considerably lighter in weight than it entered. The next process the roll of foil undergoes is called the formation process. Aluminum oxide is grown onto and into the hollow tunnels which were etched into the aluminum during the etching process. Figure 4 shows the scanning electron microscope edge view of a sheet of the oxide tunnels after the surrounding aluminum was dissolved and a closer view of some oxide tunnels. Notice that the inside diameter of this 550-volt oxide tunnel is about a quarter of a micrometer and that the wall thickness is a little more than one-half micrometer. In general, the ratio of the oxide thickness to the oxide formation voltage is about 1.0 nanometer per volt. This ratio varies somewhat with the oxide structure. Depending on the formation electrolyte composition, the current density, and other production parameters, the structure of the aluminum oxide may be amorphous, crystalline, hydrous, or some combination of these structures.

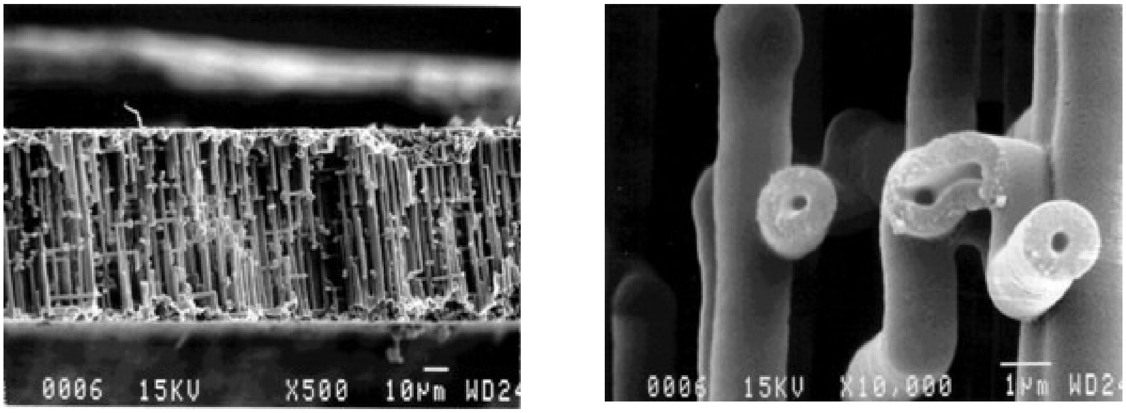

Fig. 4. Scanning electron microscope edge view of a sheet of the oxide tunnels after the surrounding aluminum was dissolved (left), and a closer view of some oxide tunnels (right).

The etching and forming processes must be compatible to achieve good results. Figure 5 shows a cross-section of a tunnel in the anode aluminum before and after forming. Note that the relationship between etched tunnel diameter and the formation voltage (thickness) is important. Since the oxide grows inward as well as outward in the tunnel, if the etch diameter is too small, the tunnel can clog or completely fill with aluminum oxide during the formation process, thus contributing little to the foil capacitance, since the electrolyte cannot contact the inside of the tunnel. If the tunnel diameter is too large, the optimum capacitance cannot be realized due to wasted space. The combination of the etching and forming processes determine the formation voltage "V_f" and the gain of the foil produced. The gain is defined as the capacitance per unit macroscopic area of the produced foil divided by the capacitance per unit area of unetched foil of the same formation voltage. High energy density aluminum electrolytic capacitors use high-gain foil. It may be noted here that the breakdown field strength of 1 V per 1.0 nm is much higher than for polymer films. The "k" value of 8.5 for aluminum oxide is also about three times larger than for most film dielectrics (see Table I). Aluminum oxide is several times denser than polymeric films, however.

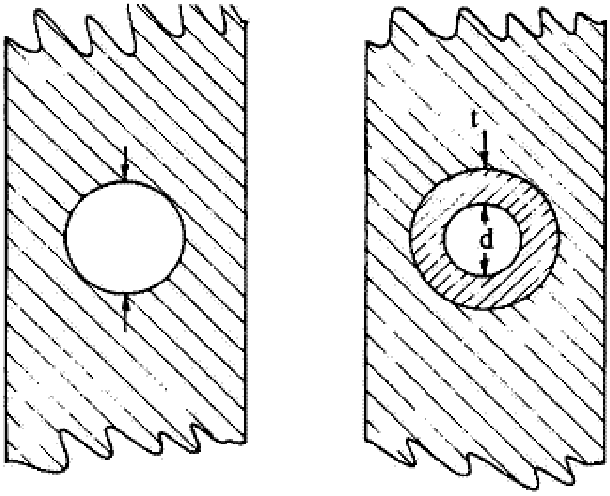

Fig. 5. Anode tunnel cross-section before (left) and after (right) the oxide formation process

Cathode

The cathode aluminum foil is generally thinner than the anode and must exhibit much higher capacitance than the anode, since the cathode capacitance appears in series with the anode capacitance to yield the total capacitance. For a given anode capacitance, the maximum total capacitance occurs when the cathode capacitance is as large as possible. High cathode capacitance requires a very low cathode formation voltage. Generally the cathode is not formed at all, but there is always a thin layer (around 2-3 nm) of hydrous oxide on the surface of aluminum unless it is passivated and the electrical double layer also has a large capacitance. A thin hydrous oxide layer forms readily on aluminum with exposure to normal air in the atmosphere. Titanium passivation of cathode foil has been undertaken in recent years to offer a cathode with a capacitance approaching 200 $\mu F/cm^2$. Such a high cathode capacitance is necessary only for low-voltage capacitors with high-gain anodes. Generally a cathode capacitance of fifty times the anode capacitance is sufficient. This situation yields a total capacitance which is only 2% less than the anode capacitance. For a discharge capacitor, the charge on the anode plate must be neutralized by the opposite charge on the cathode plate, which requires that the cathode be capable of storing a charge greater than or equal to the anode charge. In other words, the product of the capacitance and forming voltage must be larger for the cathode than for the anode. This requirement is generally met automatically, since the charge storage capability of formed foil is maximized at low formation voltage. A thin foil with a surface etch is used for the cathode, giving a frequency response generally better than that of the anode, and giving a large enough capacitance that the total unit capacitance is not diminished. Since the cathode's voltage capability is usually only about one volt, the electrolytic capacitor unit is limited in its steady-state reverse voltage capability to about one volt. It has been found that in some cases transient reverse voltages in excess of 100 volts may appear on the capacitor for durations of around one millisecond with no detrimental effects for thousands of cycles; however it is not clear what the actual cathode potential is in these cases. What is known is that extended reverse voltage for time intervals as short as one second can cause significant heating of the electrolyte and of the anode oxide. The current drawn during these reverse voltages can easily reach hundreds of DC amperes. Electrolytic capacitors can be constructed with formed cathodes to allow voltage reversal without damage. The drawbacks to such construction are reduced total capacitance, since the anode and cathode are in series; and reduced energy density, due to the decreased capacitance and increased mass from the heavier, formed cathode.

Separator

The separator or spacer is an absorbent material in roll form which is wound between the anode and cathode to prevent the foils from coming in contact with one another. The spacer is generally made of paper, which can be of many different types, densities, and thicknesses, depending on the voltage and effective series resistance requirements. Besides separating the anode and cathode, the spacer must wick and hold electrolyte between the plates. The resistance of the spacer-electrolyte combination is appreciably greater than would be accounted for by its geometry and the resistivity of the absorbed electrolyte. The electrolyte-spacer combination also impacts the capacitor's frequency response.

Electrolyte

The primary purpose of the electrolyte is to serve as a "plate" on the outer anode oxide surface and also to connect to the cathode plate. The electrolyte is a high-resistivity, high-dielectric-constant, high dielectric-strength organic liquid solvent with one or more dissolved, ionically conductive solutes. The secondary purpose of the electrolyte is to repair, heal, or insulate defect sites in the anode aluminum oxide during the application of voltage between the anode and cathode.

Tabs

Tabs are strips of aluminum which make contact between the conductive plates and the connection terminals in the header. There may be several tabs connected to each of the plates. Each tab is either cold-welded or staked along the entire width of the anode and cathode foils. The tab paths are generally run from the capacitor section to the terminals in a fashion which keeps the inductance low and prevents tabs of the opposite polarity from coming in contact with one another or the case during movement and vibration of the capacitor unit. The tabs are spot-welded to the underside of the terminals in the header assembly. Tab material is not etched, but is formed to a high voltage prior to its assembly into a capacitor. Optimum tab placement along the foil is considered to be the placement that minimizes power loss due to the metal foil resistance. This optimum leads to equal spacing from each tab to the one nearest it, and half of the inter-tab distance is provided between the outermost tabs and the foil ends. For high voltage capacitors, the tab resistance and metal foil resistance are quite small compared to the oxide and electrolyte resistance.

Package

The can into which the capacitor section is placed is made of 1100-alloy aluminum, which is of around 99% purity. For 25 to 50 mm (one-inch to two-inch)-diameter capacitors, the wall thickness is 0.022 inches. A butyl rubber gasket is placed on top of the header before the spinning operation, in which the case opening is folded over and pressed into the gasket, forming an effective seal of the system. The package is at the same potential as the electrolyte and cathode during capacitor operation, so when electrolytic capacitors are connected in series, care must be taken to insulate the cases from one another. Although the aluminum electrolytic capacitor case is at the cathode potential, it may not be used for the negative electrical connection because of high electrolyte resistivity and the long effective path from the cathode to the can. If the electrolyte were of much lower resistivity, eliminating the cathode and using the can instead might be a possibility. A safety vent is provided in capacitors so that the capacitor may relieve excessive pressure buildup in a controlled manner. This occurrence is known as venting, and is considered a failure mode. The vent may be installed as a rubber plug in the header or as a die-set slit impression in the can wall. The pressure at which the capacitor vents is predictable, and is usually designed to occur at about seven atmosphere pressure or even higher. The allowable pressure tends to be higher for small capacitors. After a capacitor vents, the electrolyte may evaporate out until the capacitance diminishes.

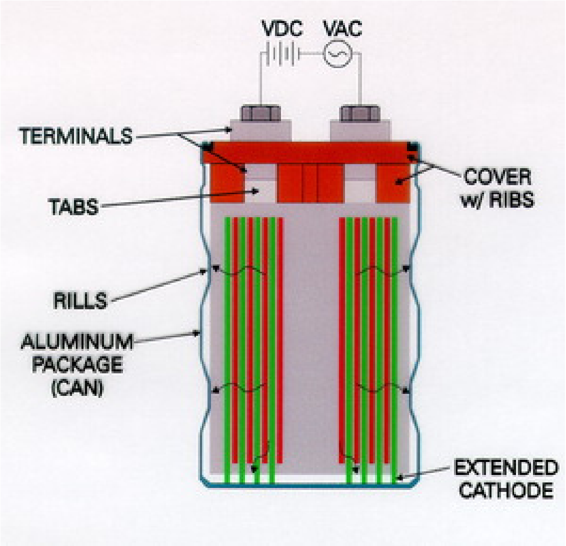

Fig. 6. Schematic of the capacitor package.

Uses and applications of electrolytic capacitors

There are many practical, everyday applications of aluminum electrolytic capacitors. The most important applications include filter capacitors for power supply outputs, blocking and DC-bypass circuits, motor start and other non-polarized capacitors, audio applications, energy discharge capacitors, photoflash and strobe capacitors.

Total worldwide usage of capacitors is approximately one trillion units per year. The total market value is approximately 17 billion dollars per year. Figure 8 show the monthly fluctuations of the total capacitor market for a couple of recent years. And Figure 9 presents the annual markets for aluminum and tantalum electrolytic capacitors, which are more than 10% of total usage

Fig. 7. Some electrolytic capacitors

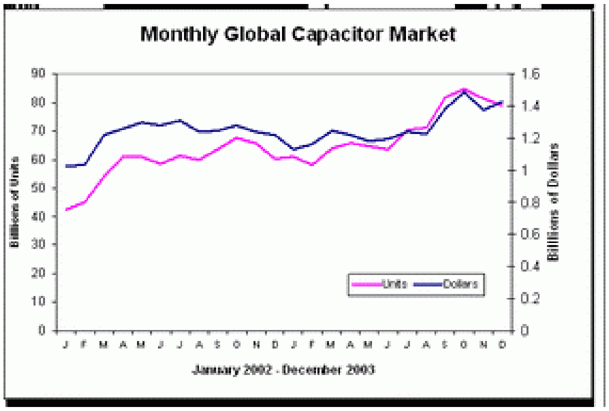

Fig. 8. Monthly global capacitor market.

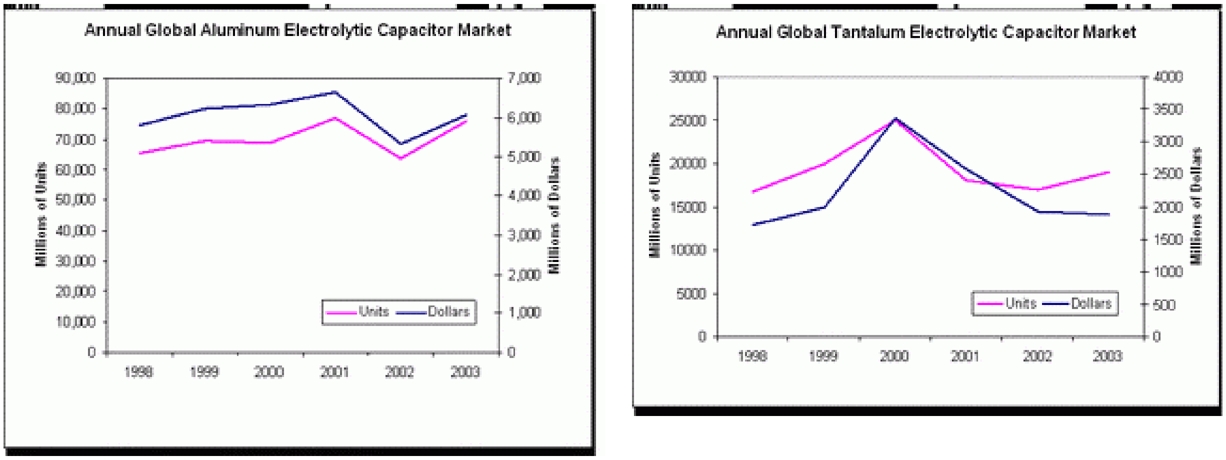

Fig. 9. Global electrolytic capacitor market: aluminum (left), tantalum (right).

III - The Etching of the Aluminum foil

The above descriptions about the electrochemical capacitors technology demonstrate that the key step influencing the performances of the device is the etching of the Aluminum foil. Thus, in this work, the attention will be focused directly oin this manufacturing step.

High surface area electrodes for aluminum electrolytic capacitors usually are fabricated with DC etching method. Aluminum anode dissolution occurs preferentially in the (100) direction, so the basic structural unit is a half cubic pit [A14]. But after a brief time (~100 ms), the pit walls passivate and only the pit bottom continues to dissolve. Passivation of new wall surface continues at the same place as dissolution of the bottom surface, producing crystallographic etch tunnels of the order of usually 1–2 μm wide and up to 50 μm long and with 10^7 cm^{-2} density [A2,A5,A10].

Part I

PIT NUCLEATION BEHAVIOUR

The capacitance of the etched aluminium foil used in electrolytic capacitors is determined by its surface area. The methods of etching are selected according to the forming voltages. DC etchings are usually adopted for the anode foils of high voltage capacitors. It is important for determining the etching mechanism to investigate the nucleation processes of pit formation.

The electrode potential of high purity aluminium foils for electrolytic capacitors moves from a high potential period to a steady period during the early stage of DC etching in a hot HCl solution. In this “Part I”, the behavior of pit nucleation was investigated. Pits varied in structure from a hemispherical pit to a half-cubic pit. The difference in the number of initial pits affects the size of the half-cubic pits and the period of pit formation during the early stage up to steady potential period.

1 - Early pit formation [A8]

Metal dissolution from pits occurs at a constant apparent current density of about 6 A/cm^2. However, the pit sizes at early times show that the equivalent current density of initial pit growth is over 100 A/cm^2. Comparison of pit volumes to charge passed confirmed that initial growth was unaccompanied by faradaic charge. However, for foils which had not been pretreated by immersion in 1N HCl at 25°C an equivalent charge was passed during early pit growth.

In the following experiment conducted by Wiersma and Herbert [A8], pitting was initiated through application of anodic current to aluminum electrodes in aqueous HCl solutions at 65°C for times ranging from 1 to 100 ms. Measurements of the potential transient at these early times were accompanied with geometric measurements of etching structures using scanning electron microscopy (SEM). Faradaic current and charge were compared to the total surface area and volume of all pits on the surface. The objectives were to identify sources of current and determine metal dissolution rates during early pit growth, and thereby gain insight into the process of pit initiation.
Etch tunnels are corrosion pits which are characterized by high aspect ratio of length to width (as much as 100 μm length to 1 μm width), and orientation along the <100> crystallographic directions. The number density of tunnels is greater than 10^5/cm^2 of metal surface. At the etch times of less than 1 s of interest in the work of present chapter, only cubic crystallographic pits are found on the Al surface.

Prior to etching experiments, the foil was pretreated by immersion in aqueous 1N HCl at room temperature for 5 min. This pretreatment had been found to promote a high density of pits and tunnels. Etching experiments consisted of constant current pulses of times less than 100 ms.

1.1 Potential transient

Potential transients during etching experiments are given in Fig. 1. Prior to etching, Al was at the open-circuit potential, which was between -0.8 and -1.0V. For the pretreated electrode at applied current 12.89 mA/cm^2, the slope of the potential transient changed at 35 ms from -190 V/s to about 0 V/s in a time of less than 5 ms. Figure 1 also shows transients for experiments with no pretreatment and with another applied current.

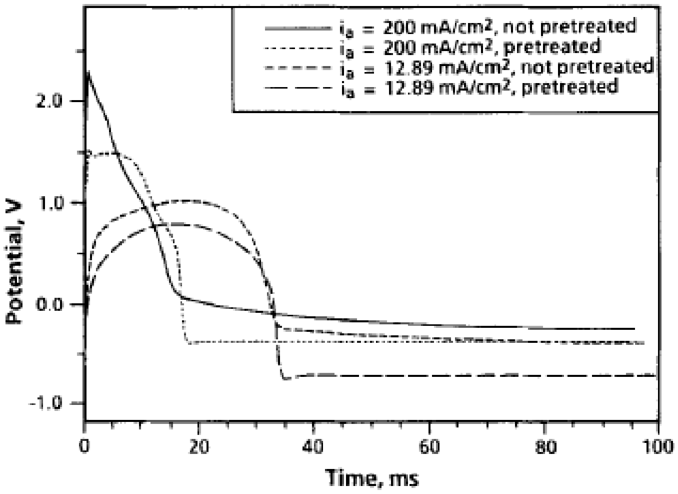

Fig. 1. Potential transients during etching experiment. Temperature 65°C, etchant 1*N* HCl. Reference electrode Ag/AgCl/4*M* KCl.

1.2 Pit morphology and distribution

Pit orientation is determined by the Al crystal structure and all pits were half-cubic in shape (1:0.88:0.51 = length:width:depth). There were also pits which were irregular in shape.

The average pit depth is 0.19 μm. No pits smaller than 0.05 μm in depth could be found. Pit densities are sho in in fig 6.

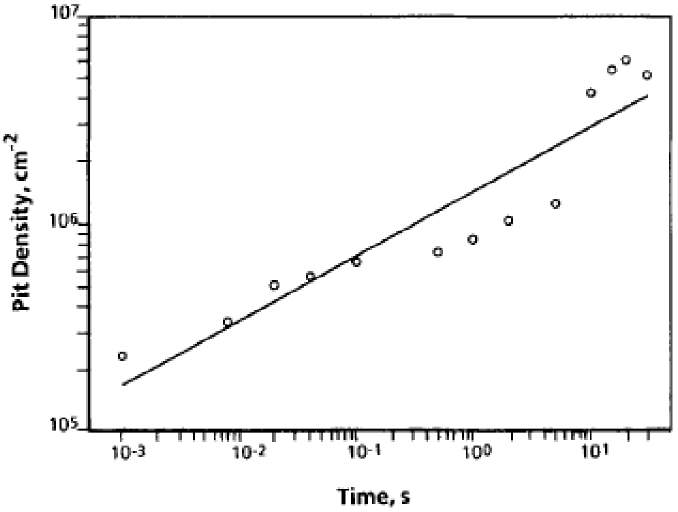

Fig. 6. Pit number densities during etching. Temperature 65°C, etchant 1*N* HCl, applied current density 12.89 mA/cm^2. Pit number densities have been corrected by subtracting number of pits formed at open circuit. Solid line is linear least squares fit to experimental pit densities.

1.3 Pits formed at open circuit

When pretreatment was followed by a 5 s dip in the etchant solution with no applied current, the pit density measured was 3.4×10^5 cm^{-2}. This immersion time is the same as the total time for which the Al electrodes were immersed in the etchant solution in etching experiments. After the pretreatment alone, the pit density was 3.4×10^4 cm^{-2}. Therefore, most of the pits found after the pretreatment and dip in the etching solution were nucleated during the brief immersion in the etching solution, during which the Al was at the open-circuit potential of -0.8 to -1.0V. This open-circuit potential is below the critical repassivation potential of -0.748V *vs.* Ag/AgCl/4M KCl, which was determined from the zerocurrent intercept of the cathodic scan in the current-potential curve shown in Fig. 5. When water was substituted for HCl solution in the pretreatment, the pit density after the pretreatment and 5 s immersion in 1N HCl at 65°C was 1.7×10^5 cm^{-2}. However, when the Al was pretreated in 1N HCl at room temperature and then immersed briefly in water at 65°C only an insignificant number of pits was observed. From these observations, it is concluded that exposure of the surface oxide film to water or 1N HCl at room temperature, followed by immersion in 1N HCl at 65°C produces the large number of pits nucleated on open circuit.

Apparently, metal oxidation during growth of the pits formed at open circuit is balanced by water or hydrogen ion reduction. For current balance calculations, it was necessary to determine whether the pits formed at open circuit were active sources of current during the etching experiments. For this purpose, potentiostatic experiments were carried out in which, following pretreatment, the Al was immersed in the etching solution and was brought immediately to a potential of -0.44V. Figure 5 shows that at the potential of -0.44V, pitting of aluminum is accompanied by a net anodic current. If the pits formed at open circuit remained active, it was expected that, when the potential was increased, hydrogen evolution would shift to the counterelectrode so that a net anodic current would accompany pitting. However, the initial current density measured in this experiment was less than 1 mA/cm^2, a value which is typical of passive current densities measured below the pitting potential. It was concluded that the pits formed at open circuit were not sources of anodic current during the etching experiments.

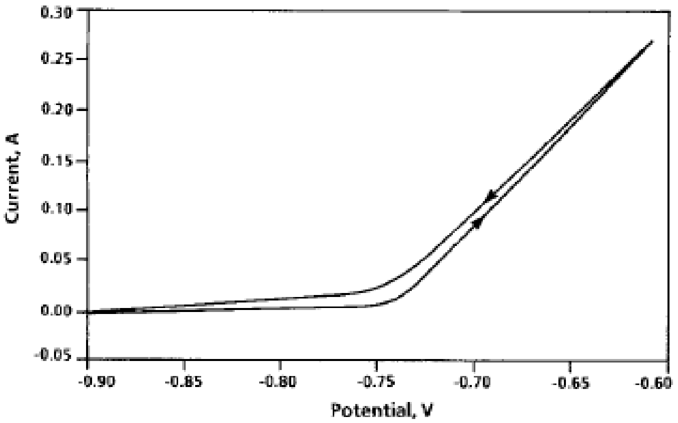

Fig. 5. Potentiodynamic polarization curve for Al in 1*N* HCl at 65°C. Potential scan rate 5 mV/s. Reference electrode Ag/AgCl/4M KCl. Electrode area 5.07 cm^2. Repassivation potential is −0.748V (zero current intercept of cathodic scan).

1.4 Current measurements

It was necessary to measure the electrode capacitance, so that the contribution of capacitive charging to the applied current could be evaluated. The value of the capacitance measured with a capacitance bridge at the open-circuit potential was 9.6 μF/cm^2. There is no significant variation of capacitance with potential from the value measured at open circuit. The average capacitance was 11.6 $\mu F/cm^2$.

1.5 Sources of current during etching

The faradaic currents during etching are now compared to the active pit area determined with SEM. For constant current experiments, the faradaic currents were calculated by substracting the capacitive currents from the applied currents. The capacitive current density is $C_d dE/dt$, where C_d is the surface capacitance. The active pit area was calculated using the following assumptions:

1. The pits nucleated at open circuit prior to application of etching current were not active sources of current during etching experiments, but all the pits nucleated during the current pulse were active. As discussed above, the pits formed on open circuit were not active because no significant current was measured immediately after the potential was stepped from open circuit to -0.44V.
2. No significant further pit growth took place after the etching current was turned off.

In constant current experiments, Fig. 8 shows that the faradaic current increases as a function of increasing active area. The currents also apparently increase with increasing potential. However, the galvanostatic data in Fig. 8 are only for etch times less than 20 ms. Inspection of the potential transient in Fig. 1 shows that between 1 and 20 ms, the potential increases to a maximum, but between 20 and 35 ms, the potential falls sharply with an increasingly negative slope. The faradaic current is given by i_a - $C_d dE/dt$, where i_a is the applied current density. Thus, between 20 and 35 ms, the faradaic current increases with time; between 20 and 35 ms, both the faradaic current and the pit area increase with time, while the potential decreases. The faradaic current is an increasing function of the active pit area, and does not depend on the potential.

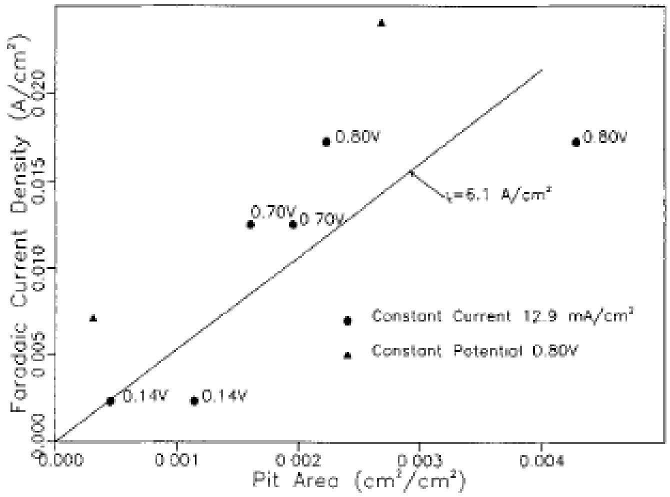

Fig. 8. Comparison of overall faradaic current per unit electrode surface area with total pit surface area per unit electrode surface area. Temperature 65°C, etchant 1*N* HCl. Solid line represents the predicted faradaic current for a constant metal dissolution current density 6.15 A/cm², and a constant current efficiency 115% (values obtained in tunnel etching experiments).

The solid line in Fig. 8 represents faradaic currents calculated by multiplying the active pit area by this tunnel current density and dividing by the current efficiency of 1.15.

This calculation is based on assumptions about the faradaic current which are now discussed:

1. Sources of faradaic current other than metal dissolution from pits and cathodic hydrogen evolution are neglected.
2. The metal dissolution current density is constant in all active pits.

The dissolution current density in the small etch pits is not appreciably different from that measured in tunnels. Figure 9 shows the dependence of the active pit area on etch time.

$$i_a = C_d\, dE/dt + A(t) i_t/\varepsilon$$

In this Eq., i_a is the applied current density, C_d dE/dt is the capacitive charging current, A(t) is the total active area in pits per unit electrode surface area, i_t is the dissolution current density in tunnels, 6.1 A/cm^2, and ε is the current efficiency for metal dissolution, 1.15. The agreement between the areas calculated from SEM measurements and the potential transient is good.

Based on Fig. 9, the following interpretation of processes occurring during the first 35 ms of applied current can be given: pits nucleated under the influence of the current at an average rate of $1.4 \times 10^7/cm^2$-s. The total metal dissolution current increased with time along with the pit density. The difference between the metal dissolution current and the applied current was supplied by capacitive charging current; the capacitive current was anodic before 15 ms, and cathodic between 15-35 ms, during which time the metal dissolution current exceeded the applied current. After 35 ms, because dE/dt is zero, the system current is controlled by controlling the metal dissolution current from pits. Control of the pit current after 35 ms may be achieved through passivation.

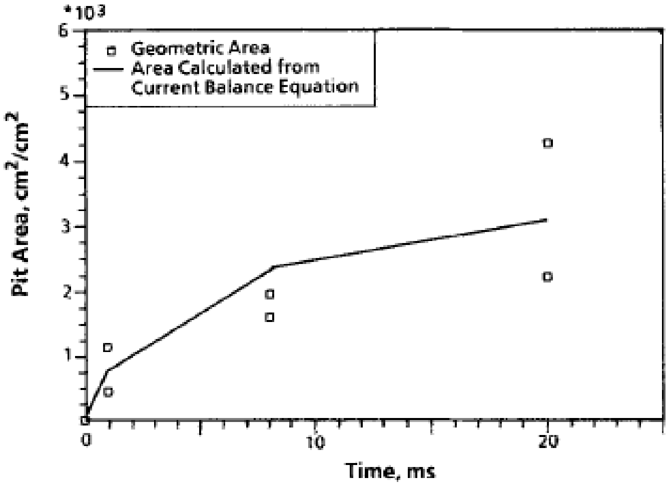

Fig. 9. Comparison of active areas measured with scanning electron microscopy with active areas calculated from potential transient using current balance equation. Temperature 65°C, etchant 1*N* HCl, applied current density 12.89 mA/cm².

1.6 Comparison of geometric pit volume and faradaic equivalent volume

It was noted above that no pits smaller than 0.05 μm were observed in the etching experiments. If pit growth to this depth takes place during a 1 ms current pulse, the average effective dissolution current density during this period is

$$(3F\rho/M_w)(5 \times 10^{-6}\ \text{cm}/10^{-3}\ \text{s})$$

where F is Faraday's constant, ρ is the density of Al, 2.7 g/cm^{-3}, and M_w is the molecular weight of Al, 27 g/mol. The calculated current density is 150 A/cm^2, 25 times larger than the current density of 6 A/cm^2 obtained above. Apparently, the nucleation of a pit is followed by a period of very rapid growth to a size on the order of 0.1 μm.

The total volume of metal dissolved from pits in a given etching experiment could be calculated from the pit size distributions

$$V = 4n_t \langle r^3 \rangle$$

$\langle r^3 \rangle$ is the mean cube pit depth. The pit volume was compared to the faradaic equivalent pit volume calculated from the total anodic charge passed during the experiment, assuming three electrons were passed per Al atom dissolved

$$V_{far} = \varepsilon\ [i_a t - C_d(E - E_o)]\ M_w/(3F\rho)$$

The samples which had been pretreated still show a geometric volume which is significantly larger than the faradaic equivalent volume, but for those which were not pretreated, the equivalent volume is close to the geometric volume.

Metal dissolution during early pit growth is primarily unaccompanied by electrode current when the Al had been pretreated, but an equivalent current is passed when there was no pretreatment.

Water or 1N HCl immersion at room temperature prior to etching produces a high density of etch pits at open-circuit conditions in the etchant solution. These pits formed at open circuit could be produced by a similar mechanism to those formed by currentless dissolution under applied current.

One possible hypothesis to explain rapid initial metal dissolution in pits is that, when the pit surface is first generated, the corrosion rate is very high because the surface is unfilmed.

6 A/cm^2 represents the true metal dissolution current density in pits. If this is the case, the early pit growth would be contributed by an additional process which operates in parallel with anodic dissolution from pits. This additional process would be currentless on pretreated surfaces, but otherwise faradaic. The parallel oxidation process may be related to the reaction between aluminum and water:

$Al + 2H_2O \rightarrow AlOOH + 3/2\ H_2$

AlOOH is a solid film material. The reaction would be expected to take place uniformly across the metal surface at the metal/film interface. It is possible that the pretreatment incorporates water in the film, so that this reaction can occur. As the Al metal atoms are oxidized into the film as a result of this reaction, they may leave behind vacancies in the metal. The vacancies could in turn diffuse through the metal to growing pits. Vacancy diffusion would then account for the early pit growth.

2 - Early pit growth and hydrogen transportation out of the pit [42]

Hydrogen with nanometer size can be absorbed on the sidewalls' surface of a tunnel; the area containing saturation hydrogen is formed at the end of a tunnel, and the saturation hydrogen can accumulate to form a large bubble before the hydrogen is transported out of the tunnel; the large hydrogen bubble will emanate from the end of tunnel when the pressure in the bubble is equal to the pressure out of the tunnel.

Fig. 7 shows the schematic diagram for hydrogen bubbles to transport out of the end of a tunnel. Fig. 7a–c shows that the pit is formed and gradually develops to be a hemispherical pit because the dissolution velocity is same at every direction

Some small hydrogen bubbles are absorbed on the sidewalls of a pit when the size of the pit grows big enough as shown in Fig. 7c. The area containing saturation hydrogen is formed when the number of small hydrogen bubbles is big enough at the end of tunnel, then a large bubble is formed. Consequently, the large bubble will emanate from the end of tunnel when the pressure in the bubble is equal to the pressure out of the tunnel.

Aluminium anode dissolving begins when the hydrogen bubble leaves the mouth of a tunnel and the elctrolyte enters into the end of the tunnel.

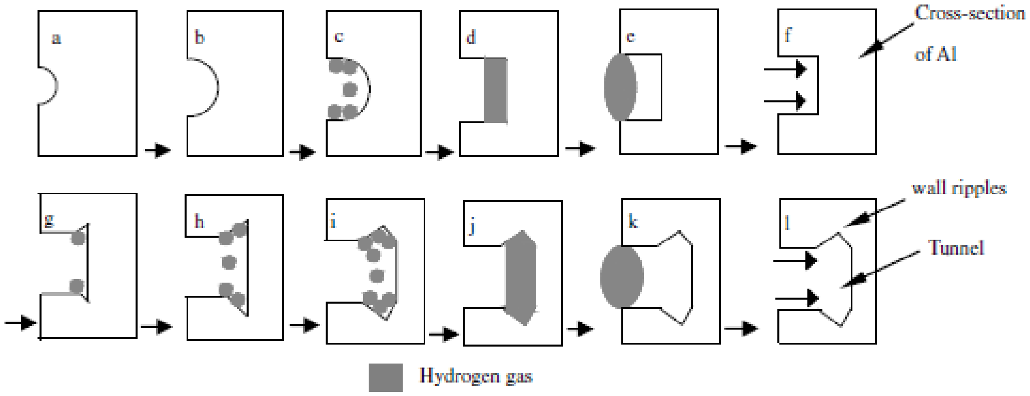

Fig. 7. Schemes of the pulse electrochemical etching process.

3 - Trace elements' effects

3.1 Effect of Ti, Mn, Fe, Si, Cu [A1]

Within the range of the commercially produced alloys the influence of a variation of the Mn, Ti and Cu content can be evluated.

The most significant influence of the composition seems to be the Cu-content: this influence is more or less linear.

The capacity of the foil is influenced by the composition of the foil, the dispersion of second phase particles and to a smaller extent by the grain size.

Mn has no influence; an increase of the Ti content from 0.01 until 0.1% increases the capacity by 13%; an increase of the Cu-content from 0.01 to 0.2% increases the capacity by a factor 3.

Various kind of precipitates may be formed as a function of the aging time and temperature after a previous homogenizing and quenching treatment.

The beaviour during the aging of the "high copper alloys" (Al 3.6% Cu alloy) presents a representative example.

A prolonged aging treatment, or an aging treatment at higher (> 90 °C) temperature, which produces a large numbers of coarse precipitates (partly at the grain boundaries) leads to catastrophic results with regard to the capacity: a factor 3 less than the maximum capacity of this Al 3.6% Cu alloy.

Can be concluded that etchability and capacity is improved by the following three factors:

- a small grain size
- a fine dispersion of precipitates
- a high copper content

The most important variable still seems to be the Cu content. The higher the copper content is, the higher the capacity will be. It is in agreement with the fact that the pitting potential becomes less negative with increasing Cu content, so it can be said the pitting potential becomes less negative with increasing capacity.

Prolonged aging of the material will cause the precipitation of Cu-rich particles and the Cu-content of the matrix will decrease corrispondingly.

As a result the pitting potential also decreases. Still the capacity increases with precipitation.

3.2 Effect of Bismuth and Boron

Araki, Suzuki and Atsumi [A1] found that trace bismuth or boron in aluminium greately influenced etching morphology.

Etching was electrolytically performed and finally capacitance was measured. Two steps of DC electrodyc etching in 7% HCl solution were used. Temperature was 353°K for the first step and 363°K for the second. These conditions were selected to gain high capacitance for the particular formation voltage used. The etching time was 210 s in the first step and 420 in the second.

After the initial 30 s etch a sample labeled (α) has a relatively uniform distribution of each pits. However another sample (β) containing trace bismuth, had fewer etch pits and another sample (γ) containing trace boron, had portion of the surface with fewer etch pits and coarse surface etch morphology.

The tunneling density decreased in order from γ to β to α. On the other hand, the degree of surface dissolved was decreased in order from α to β to γ. Accordingly the capacitance of sample γ was the highest, that of sample β, containing trace boron was next, and that of sample α, containing trace bismuth, had the lowest capacitance.

4 - Pit nucleation beahviour during early stage of DC etching [A14]

4.1 Changes in electrode potential

Changes in the electrode potential of the initial DC etching are shown in Fig. 1. The electrode potential during DC etching is initially high and then becomes steady with a transition period of up to a few milliseconds.

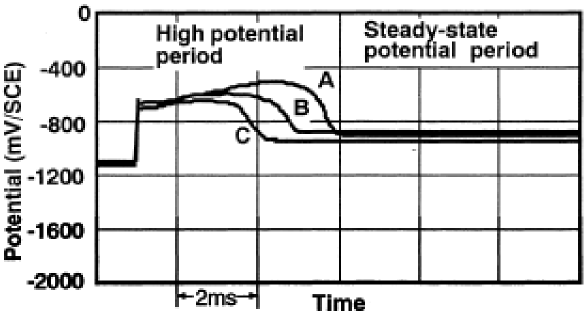

Fig. 1. Changes in electrode potentials for specimens A–C during the early stage of DC etching at a current density of 200 mA cm^{-2} in 1.5 M HCl solution at 70°C.

Scanning electron micrographs of the resin replicas obtained from specimen labeled ‘C’ after initial DC etching up to 10 ms are shown in Fig. 2. Pits varied in structure from a hemispherical pit to a half-cubic pit with a cluster of hemispherical pits. Pits with crystallographic dissolutions of (1 0 0) faces and facets are observed after a 10 ms DC etching. Other morphologies are shown in Fig. 3. Clusters consisting of multiple pits are observed after 5 ms in Figs. 2(d) and 3(a).

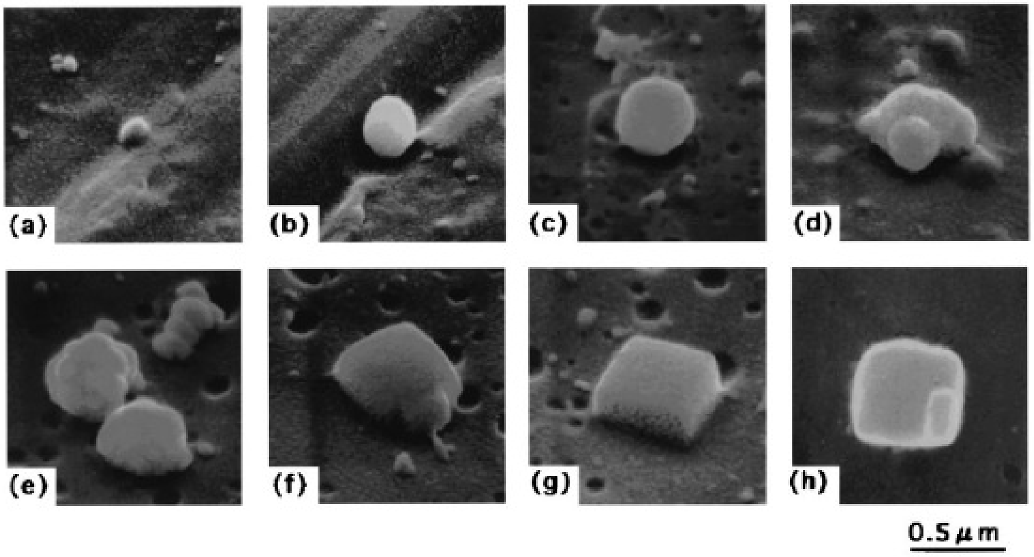

Fig. 2. Scanning electron micrographs of resin replicas obtained from specimen C etched at a current density of 200 mA cm^{-2} in 1.5 M HCl solution at 70°C for (a), (b) 2 ms, (c), (d) 5 ms, (e), (f) 7 ms and (g), (h) 10 ms. Stage tilts for all specimens are 45° except for (h), which is of 0°.

Table 1
Chemical compositions of specimens (ppm)

Specimen	Si	Fe	Cu	Mn	Mg	Cr	Zn	Ga	Ti	Pb	Al (%)
A	5	6	44	< 1	< 1	< 1	< 1	< 1	< 1	0.1	99.99
B	8	8	43	< 1	< 1	< 1	< 1	< 1	< 1	0.5	99.99
C	8	9	43	< 1	< 1	< 1	< 1	< 1	< 1	0.8	99.99

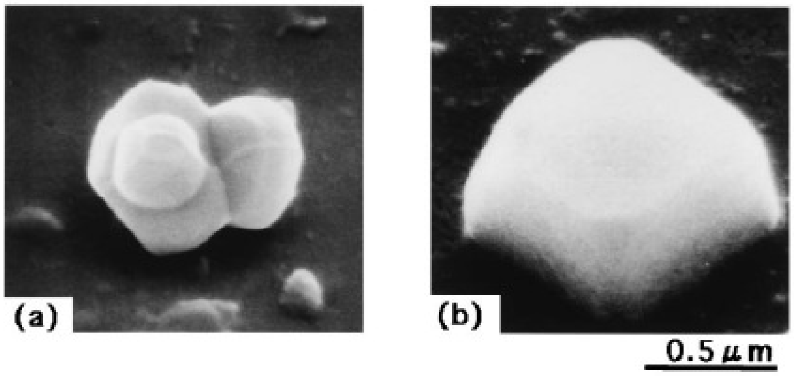

Fig. 3. Scanning electron micrographs of resin replicas showing crystallographic dissolutions of (1 0 0) faces, etched at a current density of 200 mA cm^{-2} in 1.5 M HCl solution at 70°C for (a) 5 ms with specimen B and (b) 15 ms with specimen A.

Transmission electron micrographs of the pit structure of specimen A after a 50 ms DC etching are shown in Fig. 4. Films are observed on the side walls and on part of the tip of the half-cubic pit. Judging from the result after observation of the films, it is realized that the side walls are passive, and that tunnels grow due to the dissolution at the tips of the pits. The distribution of pits after a 50 ms etching is shown in Fig. 5

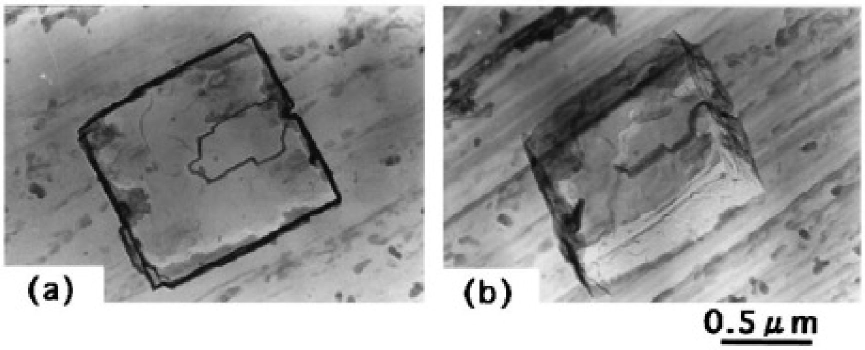

Fig. 4. Transmission electron micrographs of a film removed from specimen A etched at a current density of 200 mA cm^{-2} in 1.5 M HCl solution at 70°C for 50 ms. Stage tilts for (a) and (b) are 0° and 45°, respectively.

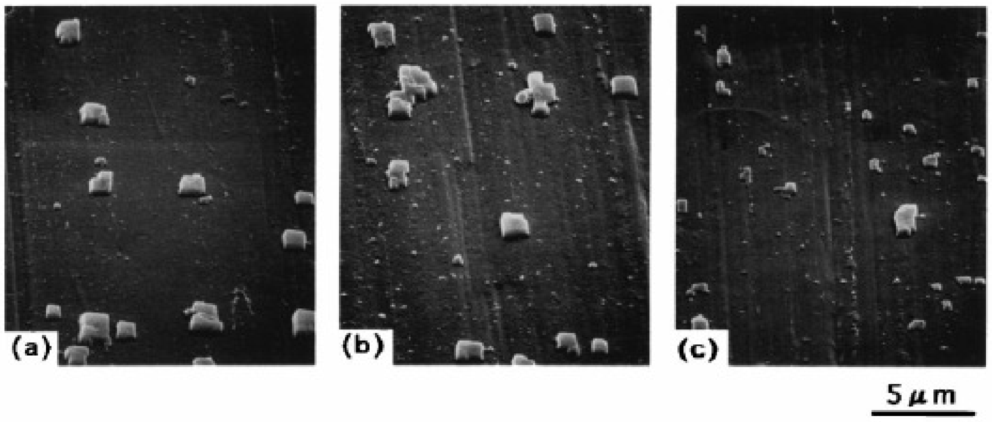

Fig. 5. Scanning electron micrographs of resin replicas showing pit distributions of (a) specimen A, (b) specimen B and (c) specimen C etched at a current density of 200 mA cm^{-2} in 1.5 M HCl solution at 70°C for 50 ms. Stage tilts for all specimens are 45°.

The current densities per one pit calculated by i/NS are (pit densities N and average pit areas S are 2.0×10^{-2} and 2.6×10^{-2}) 7.7-10.0 A cm^{-2}, where i is the current density applied, then the current densities per one pit is calculated by $(dl/dt)(z\rho F/M)$ was 8.1-9.8 A cm^{-2}.

Examples of the pit structures are given in Fig. 7. The average ratios of length:width:depth were 1:0.86:0.45 (specimen A), 1:0.95:0.45 (specimen B), and 1:0.95:0.50 (specimen C). As they are regarded as 1:1:0.5 in general, the shapes of initial tunnel pits are half-cubic. [A8]

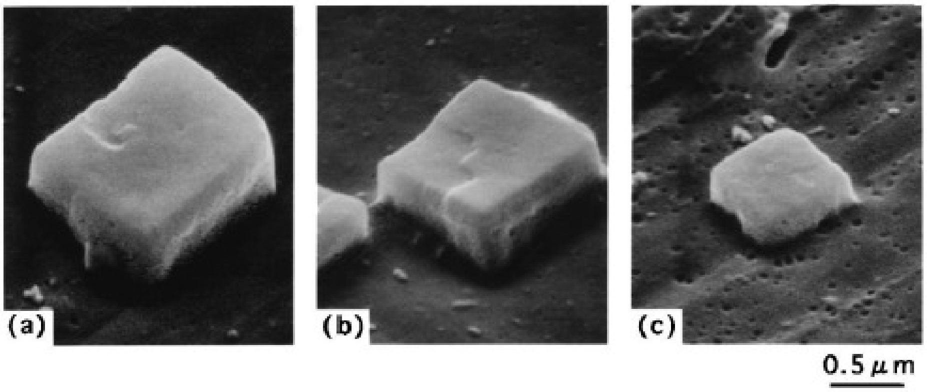

Fig. 7. Scanning electron micrographs of resin replicas showing pit structures of (a) specimen **A**, **(b)** specimen B and (c) specimen C etched at a current density of 200 mA cm^{-2} in 1.5 M HCl **solution at** 70°C for 50 ms.

Since the shapes of the initial tunnel pits are half-cubic, the radius of pit r is given as w/2, and the integrated equation is given:

$$w^2/4 = (2\ D\ C_s\ M_w\ t)\ /\ \rho$$

where:

C_S: concentration of saturated $AlCl_3$ in electrolyte (mol cm^{-3})
D: diffusivity of Al^{3+} in electrolyte (cm^2 s^{-1})
i_L: limiting current density at the mouth of a hemispherical pit (A cm^{-2})
r: radius of hemispherical pit (cm)
F: Faradaic charge
z: chemical electric charge of aluminium
M_W: atomic weight of aluminium
ρ: density of aluminium (g cm^{-3})
t: etch time (s)

The formation of a pit requires a long period with increasing size of pit, w, when the diffusion of Al^{3+} in the electrolyte is the rate determining step. Fig. 8 shows C_S plotted by using the value of concentration of saturated $AlCl_3$ in various HCl concentrations, while the temperature dependence of the solubility was ignored.

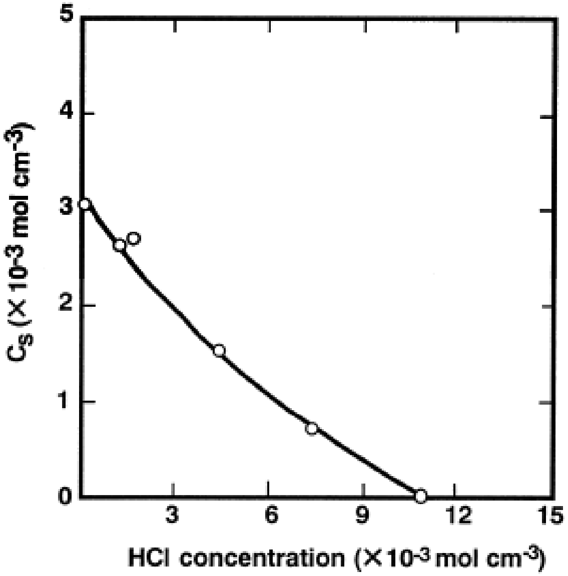

Fig. 8. Concentration of saturated aluminium chloride C_S in hydrochloric acid

4.2 Relation between pitting potential and steady-state

Anodic polarization curves of specimen A in various HCl concentrations are shown in Fig. 9. For all specimens (A-C), a good correlation between log[Cl^-] and the pitting potential is shown in Fig. 10. Pitting potentials (E_{pit}) are given as:

Specimen A: $E_{pit} = -0.901 - 0.162 \log[Cl^-]$
Specimen B: $E_{pit} = -0.932 - 0.181 \log[Cl^-]$
Specimen C: $E_{pit} = -0.942 - 0.190 \log[Cl^-]$

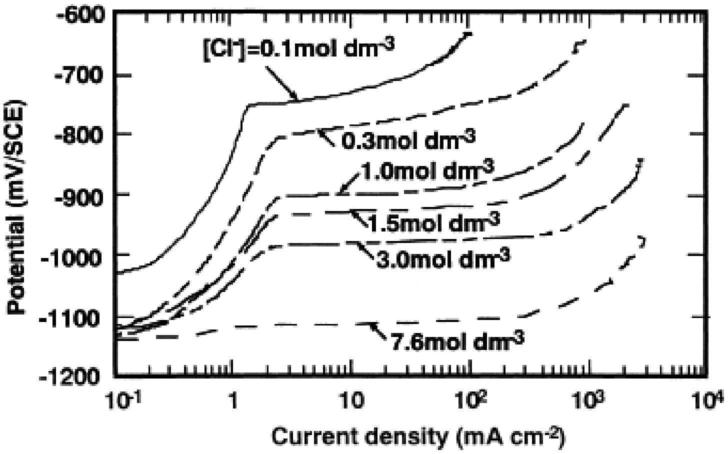

Fig. 9. Anodic polarization curves of specimen A in 0.1–7.6 mol dm^{-3} HCl solutions at 70°C with sweep rate of 50 mV min^{-1}.

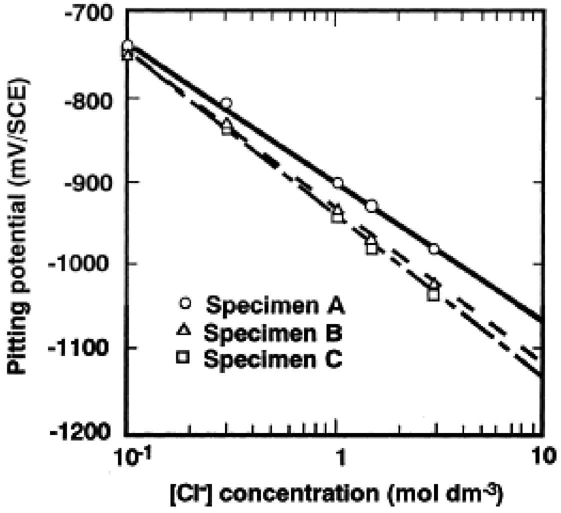

Fig. 10. Relation between Cl^- concentration and pitting potential.

Morphology of an aluminium surface after the anodic polarization (current density: 0.1 A cm^{-2}) is shown in the scanning electron micrographs in Fig. 11. Crystallographic dissolutions are randomly formed at low Cl^- concentrations. Tunnel dissolutions growing along the <100> directions perpendicular to the original surface are clearly found with increasing Cl^- concentration.

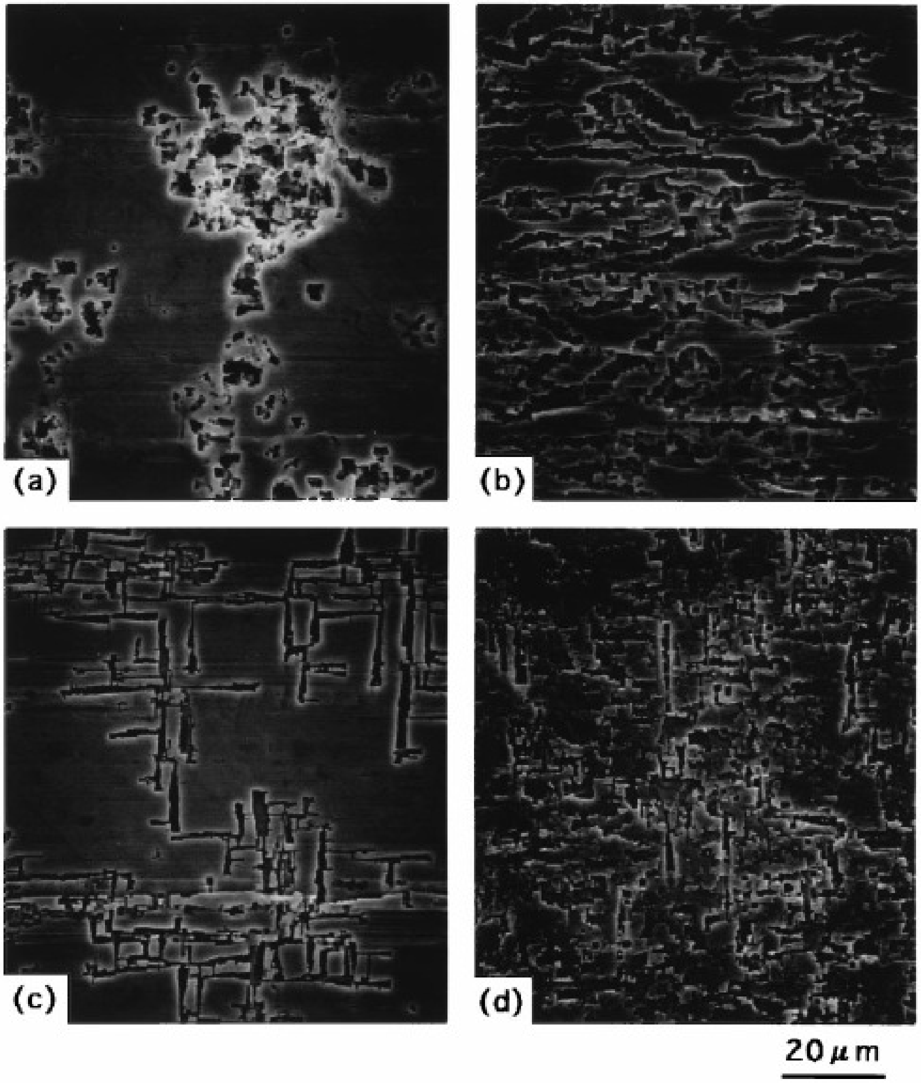

Fig. 11. Scanning electron micrographs of surfaces after anodic polarization at a current density of 0.1 A cm^{-2} in (a), (b) 0.1 M and (c), (d) 7.6 M HCl solutions at 70°C with sweep rate of 50 mV min^{-1} showing changes in structures from clusters of crystallographic dissolutions to tunnel dissolutions with increasing Cl^- concentration in the bulk electrolytes. (a), (c) and (b), (d) are specimens A and C, respectively.

The steady-state potential shifts to a less noble value with increasing Cl^- concentration similarly to the pitting potential.

The limiting current density at the mouth of a hemispherical pit, i_L, is given as:

$$i_L = 3\ F\ D\ C_S\ /\ r = 3\ F\ [\ (D\ C_S\ \rho)^{-0.5}\ /\ (2\ M_w\ t)^{-0.5}\ ] \qquad [A7]$$

5 - Salt film

The potential peak, which was observed during the early stage of DC etching, was more noble than the steady-state potential. The formation of a salt film has been discussed. It was found that a continuous aluminium chloride film was formed at high anodic potentials. The formation of a salt film is accompanied by the concentration of Cl^- and the diffusion of Al^{3+}. On the other hand, hemispherical and crystallographic dissolutions were confirmed at high potentials and at the pitting potential.

A scheme of reaction and transport for a dual salt layer on corroding aluminium is shown in fig 7. An anhydrous $AlCl_3$ layer with sinh conduction is next to the metal. An outer hydrated $AlCl_3 \cdot 6 H_2O$ layer with ohmic conduction is on the solution side. The solution next to the outer salt layer is saturated with $AlCl_3$. A small amount of water diffuses through both layers to the metal where it is discharged to form H_2 and O^{2-}. The H_2 is assumed to diffuse through the salt layers. A larger flux of water diffuses to the dual salt boundary where the hydration reaction occurs. [A3]

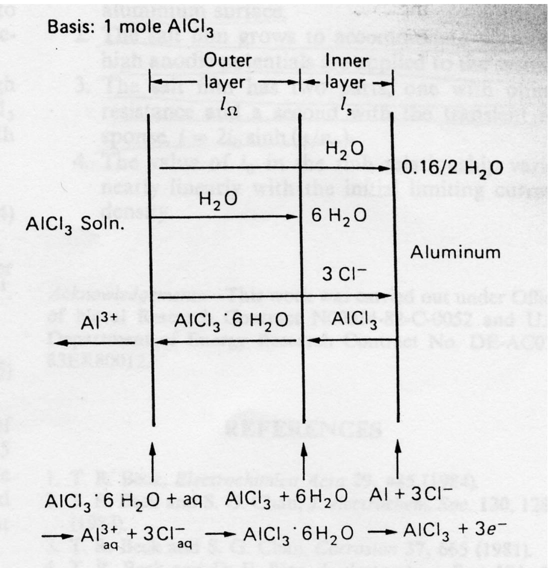

Fig. 7. Scheme of reactions and transport for dual salt layer on corroding aluminium.

The pitting potentials shift to less noble values, and the surface morphologies vary in structures from clusters of crystallographic dissolutions to tunnel dissolutions with increasing Cl^- concentration in the bulk electrolytes. The increase in Cl^- concentration also makes the high potential period short, and makes the stability potential less noble. The solubility of $AlCl_3$, C_S, is reduced with increasing HCl concentration.

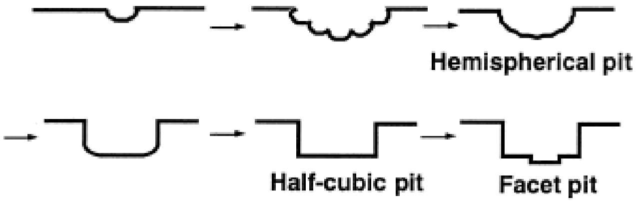

Fig. 14. Schematic diagram for change in pit structure during nucleation.

Therefore, the formation of a salt film is enhanced in a pit with the concentration of Cl^-. The high potential period is considered for pit nucleation.

As shown in Fig. 14, pits continue to nucleate within a pit or other active sites until continuous aluminium chloride films are formed. During this period, the diffusion of Al^{3+} in the electrolyte is the rate determining step. The crystallographic dissolutions of the (1 0 0) faces occur after the growth of the hemispherical pits, and then form half-cubic pits. Pits with facets grow at the steady-state potential, which is regarded as the pitting potential.

Impurities in the aluminium foils, such as indium, bismuth and so on, are also well-known to affect the etching behavior. The results indicated that the difference in the lead content affected the number of initial pits and the pitting potential during the early stage of DC etching. It appears that the lead atoms, which are distributed at the surface of the aluminium foils, provide the nucleation sites for the pitting attacks, although the lead atoms have not been directly observed by electron microscopes.

6 - Influence of Chloride ions concentration and potential [A6]

Anodic dissolution of aluminium is known to proceed with some unusual behaviours;

- passed a certain low current density (c.d.) the potential-c.d. relationship has a zero slope, *i.e.* dissolution occurs at a certain flat potential plateau at any c.d.
- anodic attack is highly localized ('pitting') and any increase in current density seems to be accompanied by a corresponding increase in the number of dissolution sites ('pits').
- Hydrogen evolution rates increases in direct proportion with the anodic current density ('negative difference effect')

When left free in the electrolyte, the metal assumes a certain potential (open circuit potential, OCP) which is more negative than the dissolution potential plateau and the dissolution is very slow. The potential plateau is identical with the pitting potential. Even when brought to the pitting potential by external means aluminium starts dissolving at the active sites only after a certain induction period. Or else, if a certain c.d. is passed, the potential initially assumes some value more positive than the plateau and it takes some time before the steady-state is estabilished at the plateau. Thus, obviously some activation process must take place. It is believed that this is closely related to the nature of the dissolution mechanism.

6.1 Experiment's results

The recorded potential-time dependences, obtained upon application of galvanostatic pulses at different current densities (fig 1) show that in all cases (except at the lowest c.d. below 50 μA cm^{-2}) a potential overshoot arises before the potential sets onto a value almost independent of current density (differences arising at the increasing current density could be well ascribed to pseudo ohmic-potential). Potential continues to increase almost linearly after charging is ended, up to a certain maximum value E_{max}, and after the maximum there is a very sharp decay down to the potential plateau. The time τ_{dec} in which the decay appears is shorter, the higher the ΔE_{max}.

At current densities larger than 30 mA cm^{-2} additional overshoots are found at very short times (about 10 ms) (fig 6).

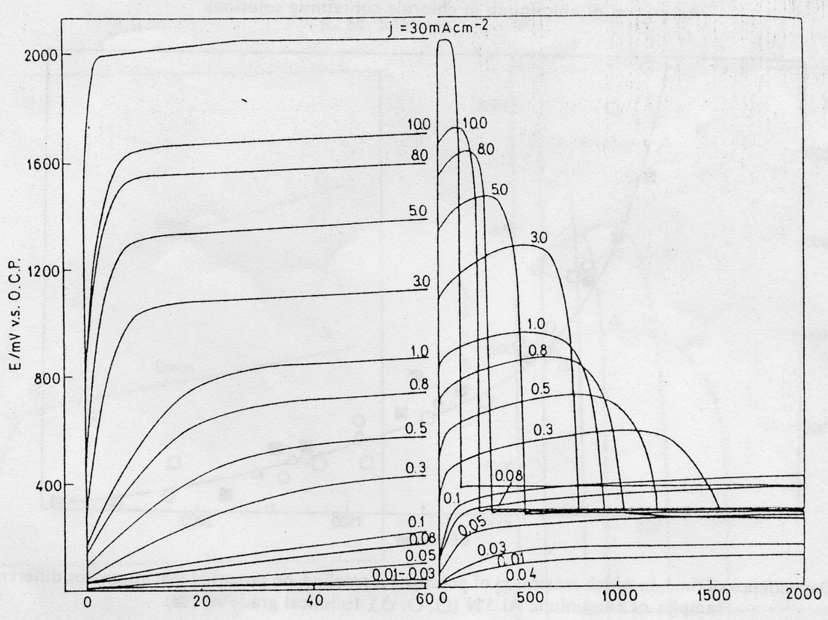

millisecondi = millesimi di secondo

Fig. 1. Oscilloscopic recordings of potential transients obtained upon application of galvanostatic pulses at different current densities.

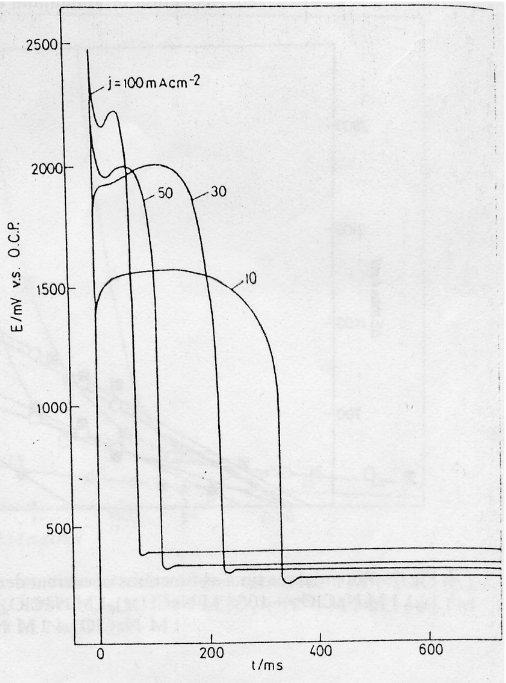

Fig. 6. Additional overshoot found at "high" current densities ($j > 30$ mAcm^{-2}).

The chloride concentration dependence was investigated by repeating the entire set of measurements in 1 M sodium perchlorate solution in which none or different amount of chloride were added to make 10^{-3} M, 10^{-2} M, 10^{-1} M and 1 M chloride solutions. The same phenomena were found in all the solutions.

Pulsating current trains were used in order to estabilish the effect of current interruption on overshoot. It is seen in fig 10 that the overshoot decreases within the first few pulse till reproducible transients are obtained. Finally it was undertaken to found the interruption period at which the overshoot vanishes. (fig 11, fig 12).

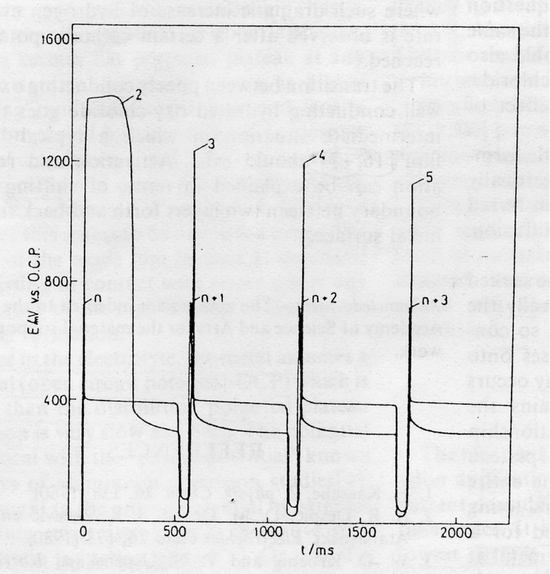

Fig. 10. Changes in the shape of the overshoot upon application of pulsating current train.

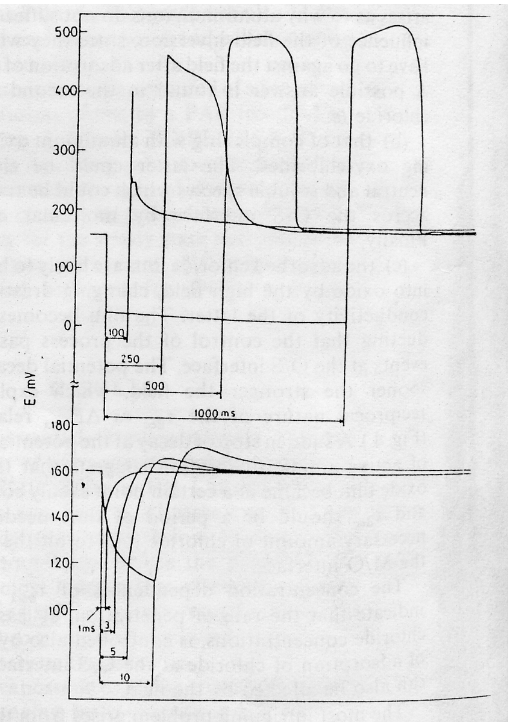

Fig. 11. Disappearance of the overshoot, at current density 3 mA cm $^{-2}$, upon shortening the interruption period.

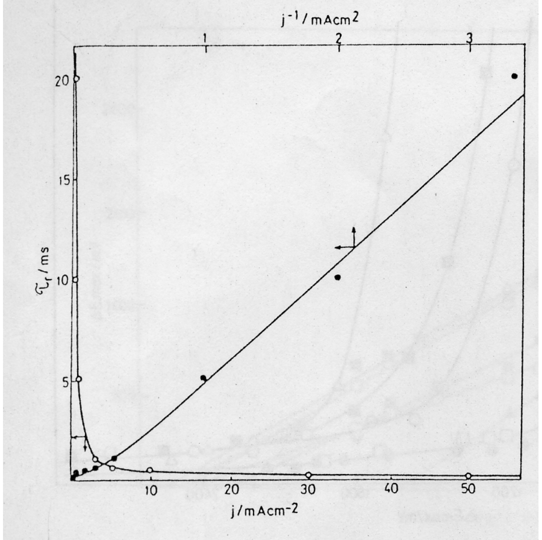

Fig. 12. Maximum of interruption time, after which no overshoot can be seen, as function of current density.

6.2 Discussion

Galvanostatic charging reflects capacitance which is smaller that the usual double layer one, and relates probably to a series of connection between the latter and the one pertaining to the establishment of the electric field across the oxide film.
The increase in E with time indicates the increase in the oxide film thickness, the rate of which should increase with increasing c.d.

The activation process of the type recorded in this experiment seems to be a general phenomenon in the anodic behaviour of metal covered by oxide film and passivated at the OCP. Activation in all these cases seems to occur when conditions are created for chloride ions to become 'adsorbed at' and 'absorbed into' the oxide film.

The induction of the positive field upon increase of potential of the metal in the positive direction in the initial period of application in the anodic current, changes the situation by allowing chloride ions to approach the O/S interface an start whatever action they can produce. There are at least three ways in which chloride could affect the process:

- specific adsorption at the O/S interface makes it negatively charged and thus inhibits charge transfer of oxigen ions from water in the oxide; the anodic potential current could be virtually cut off and the cathodic partial current should be correspondingly increased.
- Complexing with aluminium oxide forming oxy-chlorides. The latter could be electrically neutral and soluble species which could be transferred across the O/S interface by molecular diffusion.
- The adsorbed choride ions are likely to be sucked into oxide by the high field, changing drastically the conductivity of the latter. The film becomes so conducting that the control of the process passes onto events at the O/S interface. The potential decay occurs sooner the stronger the field, which explain the reciprocal nature of the τ_{dec} *vs* ΔE_{max} relationship. A sudden stop of decay at the potential plateau of active anodic dissolution suggests that the entire oxide film became at a certain

> point evenly conducting and τ_{dec} should be a period of time needed for a necessary amount of chloride ions to hit the metal at the M/O interface.

It is seen that the maximum interval of interrupting the current during which electrode remains active (in the sense that a new current pulse could be passed without any potential overshoot) decreases sharply with increasing the current density: it is like the overshoot indicates beginning of repassivation.

The most likely mechanism is not either that of a complete dissolution of the film nor that of penetrating of chloride through solid oxide. It is more likely to be somewhere in between the two, *i.e.* that action of chloride is that of complexing aluminium ions and pulling in water to hydrate the layer in a way similar to that occurring at cathodic hydrogen evolution rate is observed after a certain cathodic potential is reached.

The transition between poorly conducting oxide and well conducting hydrated oxy-chloride goes through intermediate situation in which a tipical ‘duplex film’ should exist. Activation and repassivation can be explained in terms of shifting of the boundary between two layers forth and back from the metal surface.

7 - Etching through porous alumina, pb-catalyzed [A15]

As in fig 1A, the irregularity of tunnel distribution reduces the surface area. Generally the enlarged area is below 70% of ideally expected value.

Anodic porous type alumina, which is prepared simply by the anodic oxidation of aluminium in acidic electrolytes, has arrayed honeycomb structure, as in fig. 1B.

If the ordered hexagonal array of holes in porous type alumina can be transferred to aluminium metal substrate itself by electrochemical etching, the result could be extended to make improved material for high capacitance anode of aluminium electrolytic capacitors with attractive production costs.

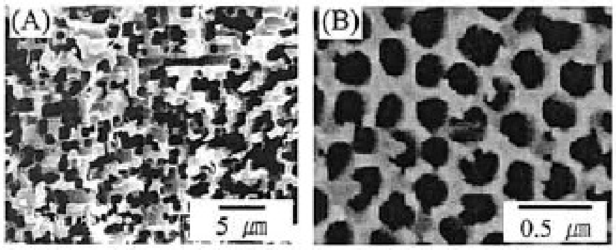

Fig. 1 (A) Random tunnel distribution on etched aluminum foil (B) Array of holes on porous type alumina.

After anodizing, the potential lowered to a pre-assigned value to weaken the barrier layer under the porous alumina. Then it was electrochemically etched in a strong acid by alternating cathodic-anodic current perturbations using a potentiostat/galvanostat.

7.1 Pattern transfer of porous alumina to substrate aluminium

Fig 2 A, shows the schematic diagrams for trasferring the array of holes in porous type alumina to aluminium substrate. By current recovery treatment after anodizing, the barrier layer thickness is reduced to the corresponding value of final potential with a small change for porous layer. And the barrier layer is mostly removed by chemical dissolution in H_3PO_4 solution. Consequently the aluminium

metal is exposed to the etching solution where aluminia holes are. Finally exagonally arrayed tunnels on the aluminium metal substrate were obtained.
The thickness of barrier layer is reduced to the equivalent value (~1.2 nm/V) for the final potential. The porous hole width increases and the barrier layer is almost eliminated by the dissolution in H_3PO_4 (fig 2 C).

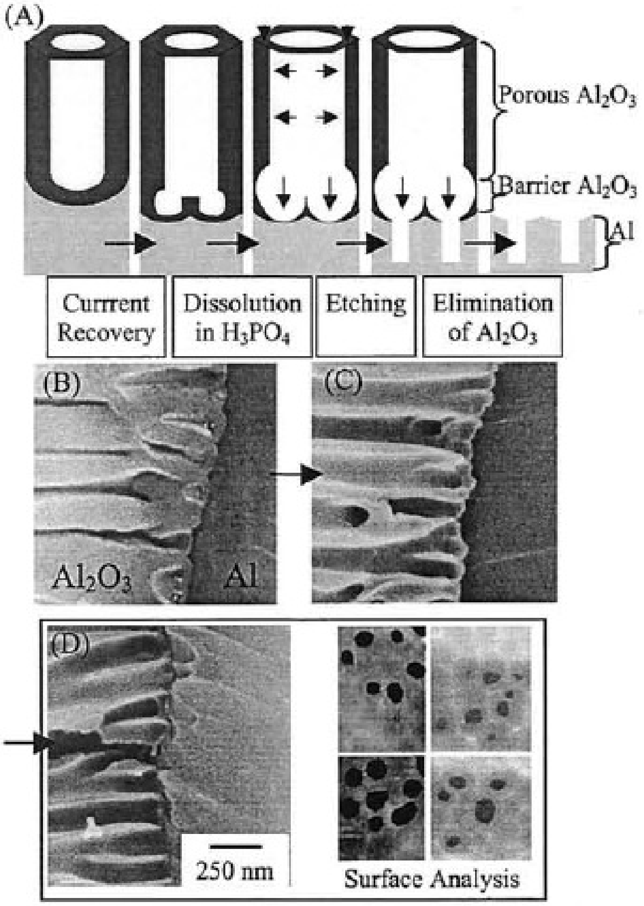

Fig. 2 (A) Outline of the procedures. (B) The cross section of current recovery treated sample. (C) After chemical dissolution in 0.4 M H_3PO_4 at 50 °C during 15 min. (D) After electrochemical etching. Right side pictures are alumina-eliminated surface.

Fig 4 shows the diminution of barrier layer thickness during the chemical dissolution after recovery treatment at various final potentials. When current recovery treatment is performed to lower final potential, the barrier layer becomes thinner.

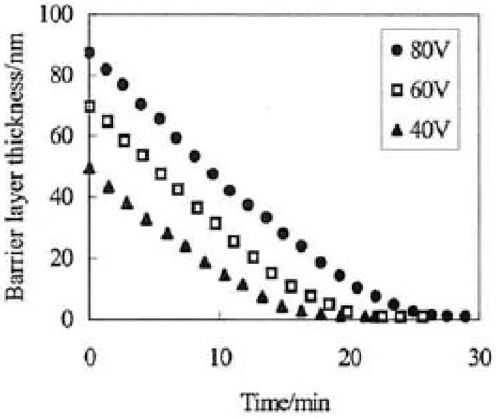

Fig. 4 Barrier layer thickness during chemical dissolution. The samples were current recovery treated from 100 V to each potential (40, 60, 80 V) before chemical dissolution.

7.2 In situ deposition of lead for cathodic tunnel etching

During the production process of aluminium foil for mid-high voltage electrolytic capacitor, about 0.5 ppm of lead is added and catalizes the tunnel initiation by Pb-Al local cells. A major portion of the lead is removed during the electropolishing. The etching speed for a pure aluminium is very slow. The presence of metals that can form a local cell is necessary to increase the etching speed.

We introduce Pb^{2+} in the etching solution and the waveform in fig 5A is applied. Lead ions in the solution are deposited where the aluminium is exposed by the cathodic pulse with the assistance of a Pb-Al local cell.

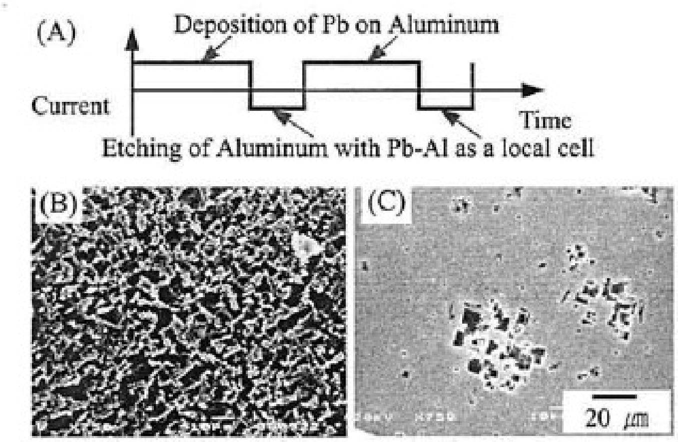

Fig. 5 (A) Waveform of engaged current (cathodic pulse: 50 mA/cm^2 during 500 msec, anodic pulse: -100 mA/cm^2 during 200 msec). (B) Etching by the waveform of (A) and Pb^{2+} in solution. (C) Etching by the waveform of (A) but without Pb^{2+}.

The deposited lead on the holes in porous alumina layer exibits stronger adherence than that on the elctropolished sample. The aluminium covered with porous alumina keeps the deposited lead with small loss during the convection and shows a distinct anodic stripping pak. These facts are applied to make effective Pb-Al local cells and to catalyze the elctrochemical tunnel etching on aluminium.

7.3 Computer simulation for the effects of preexisting ordered alumina holes

The exagonal array of porous alumina hole is partially trasferred to the aluminium substrate. If all arrays were unifomly trasferred, it will be ideal material for the low voltage (< 40 V) application. For high voltage use (> 200 V), however, the distance between neighboring tunnels must be larger that 0.9 µm considering the thickness of the indispensable barrier oxide layer that must be formed inside of each tunnel for the role of anode in capacitors. But the currently attainable maximum hole-hole distance (0.5 µm at 200 V anodizing) of porous type alumina is much smaller than 0.9. The complete transfer of the alumina holes to the aluminum substarate can result in the diminution of effective surface area due to excessively high tunnel density and their overlap.

Fig 7 shows a comparison between an industrial aluminium etching foil and that etched with porous alumina. The former (A) is electrochemically etched in H_2SO_4/HCl and it shows a typical random distribution of tunnels. The latter (B) is made by the same method as fig 2. In some area the exagonal pattern is transferred.

Porous type alumina was applied as a membrane to arrange tunnel initiation sites on aluminium in electrochemical etching. Not only uniform total transfer, but also partial transfer of equidistant alumina hole array to aluminium can increase the surface area.

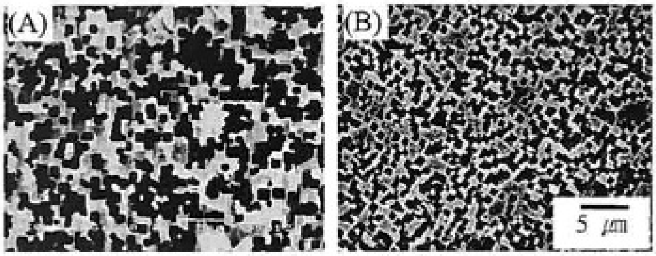

Fig. 7 (A) Industrial aluminum foil (random distribution). (B) Etched under porous alumina layer.

8 - Conclusions

The relation between changes in the electrode potential during the early stage of DC etching and pit structures have been studied.

1. The electrode potential of high-purity aluminium foils for electrolytic capacitors moves from a high potential period to a steady-state period during the early stage of DC etching.

2. Hemispherical pits occur and then grow under the diffusion control of aluminium ions in the electrolyte during the high potential period.

3. The crystallographic dissolutions of the (1 0 0) faces occur after the growth of the hemispherical pits, and then form half-cubic pits.

4. Pits with facets grow under the steady-state potential, which is regarded as the pitting potential.

Part II

TUNNEL GROWTH

During electrochemical DC etching, the etch pit width and tunnel length are influenced by the concentration of aqueous chloride [A10] and aluminum ions [E1], the electrolyte temperature [A2,A5], and the current density; the impurities in aluminum foil have great effect on tunnels' density [E2,E3]. The growth mechanism of pits was studied by many researchers, for example, morphology of the early stages of the pitting corrosion [A14,E4,E5,A16,A9], the growth model of pits about thermodynamics [A10,E6,E7,E8] and dissolution kinetics [A11,E9,E10,A13,A12,A18].

1 - Influence of Chloride ions concentration [A10]

Sulfuric acid is commonly added to the chloride etchant to control the shape of the tunnel. Data were obtained for a series with 1 N HCl and varying amounts of sulfuric acid at a fixed temperature of 77°C.

The following equation (where $\omega(x)$ is the tunnel width at depth x, and ω_0 and L are constants)

$$\omega(x) = \omega_0 \exp (-x / 2 L) \qquad (1e1)$$

was quite well followed for all compositions. The value of L decreases, *i.e.*, the tunnels taper more, as the sulfuric acid concentration increases, as shown in Fig. 6. Depth and time data for two etchants, with no H_2SO_4 and with a high concentration (7 N H_2SO_4 + 10 g/liter dissolved aluminum), are shown in Fig. 7.

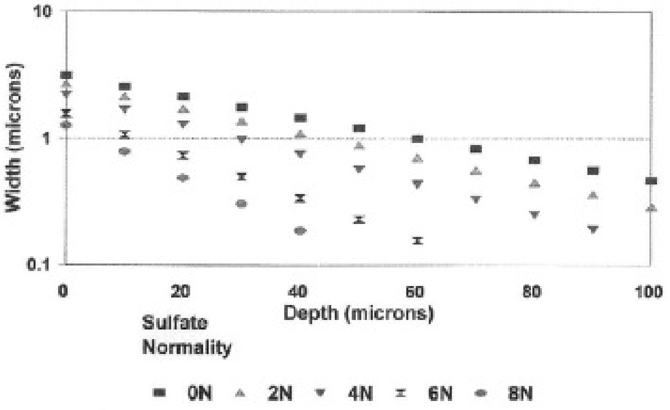

Fig. 6. Average dimensions for tunnels grown in 1 *N* HCl with additions of H_2SO_4. Each point is an average for four to eight tunnels.

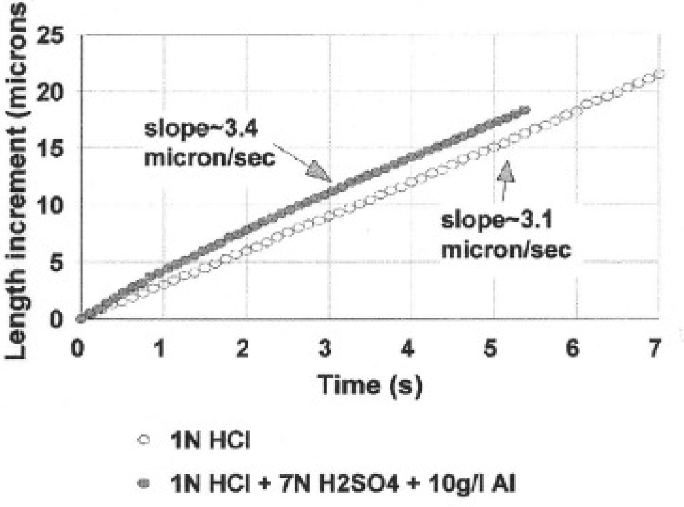

Fig. 7. Positions of maxima in tunnel width for modulated current, 200 mA/cm^2 dc + 20 mA/cm^2 ac.

The velocity values are very similar for the two solutions: values averaged over the first 5 s are 3.1 μm/s in 1 N HCl, and 3.4 μm/s for the high sulfate solution. After the first 2 s the velocities are virtually identical. The value obtained for the tunnel velocity at this temperature in 1 N HCl compares well whith a value of 2.8 μm/s. Other etchant compositions were also used. Tunnel shapes were measured for etchants containing glycerol additions . This would not be expected to have any specific chemical effect. Tunnel shapes with 20 and 40 weight percent (w/o) glycerol additions also conformed to Eq. (1e1), with smaller L values, or increased taper with higher glycerol content. Higher concentrations of HCl, with no other additions were also used. Tunnels were grown successfully in composition from 0.1 to 9 N. The L value decreases as the HCl strength increases. At the lowest HCl concentrations, the tunnels become more irregular in size and length distribution. Figure 8 shows how the maximum tunnel length varies with HCl concentration.

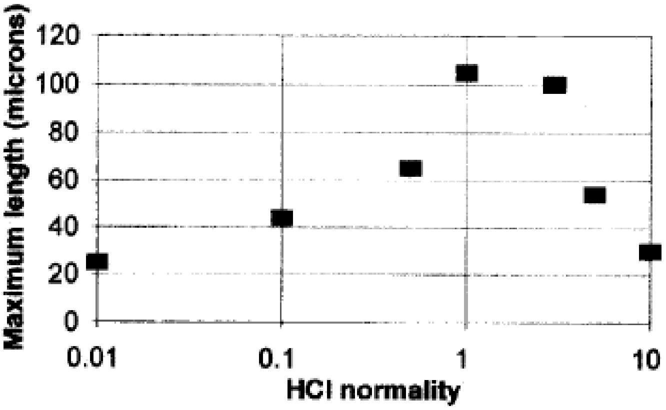

Fig. 8. Maximum length of tunnels grown in HCl at 77°C.

2 - Influence of Temperature

2.1 Influence of Temperature [A2]

The sequence of tunnel growth is illustrated in Fig. 1 for specimens that had been cleaned in NaOH and then etched at 90°C, 200 mA/cm^2. At 0.2 sec, only a dispersion of small cubic pits is present; the shallow scallops covering the surface are from the NaOH pretreatment. At 1.0 sec, the pit depth is significantly greater than width, *i.e.,* the tunnel structure has started. At 90°C and also at lower temperatures, initially only cubic pits are present and tunnels become evident between 0.5 - 1.0 s.

At 5.0 sec, tunnels are well-developed along the three (100) directions. The tunnels extending parallel to the original surface lie just under the surface and originate from a side wall of a cubic pit. Small etch pits are seen that started some time after the first

pits and will develop into later generations of tunnels. No general surface attack is evident. At 10 sec, the tunnel array has a density of vertical tunnels on the order 10^6 cm^{-2} and exhibits a range of lengths and widths. Tunnels are straight, symmetrical, and usually tapered, although parallel-sided tunnels are frequently seen. At 90°C the tunnel width at the base is generally 1.0 ~ 2.5 μm on a side, but occasionally some wider tunnels are seen. If etching at 90°C is continued, say, for 30 sec, tunnels will be 70-80 μm long and will have tapered to a width of ~0.25 μm.

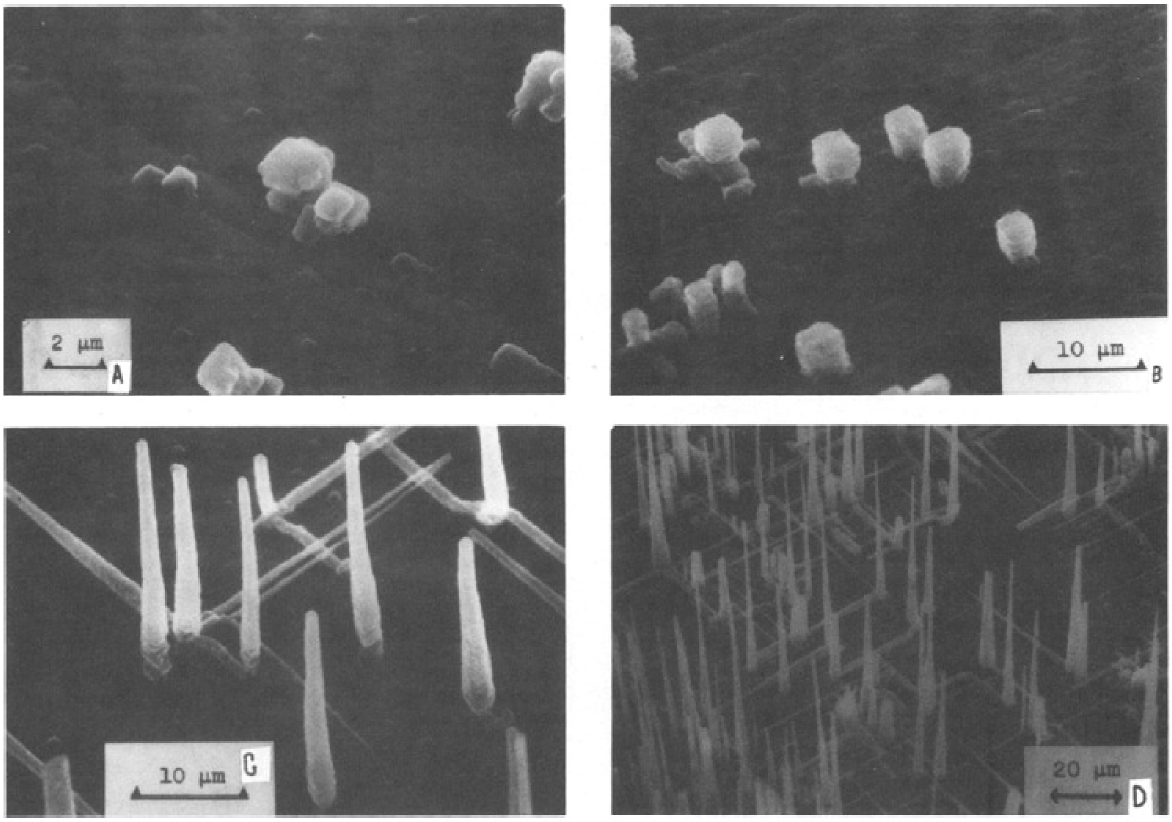

Fig. 1. Tunnel growth sequence at 200 mA/cm^2, 90°C. A: 0.2 sec; B: 1.0 sec; C: 5.0 sec; D: 10.0 sec. NaOH pretreatment

Width measurements at specified tunnel heights for short tunnels superpose similar data for long tunnels. The fact that lateral dimensions do not change with time means that all dissolution takes place at the tunnel tip. This is a critical feature of tunnel growth. Dissolution occurs in one direction and wall surfaces are passive. Figure 2 shows some structural details of tunnels grown at 70°C, 200 mA/cm^2 for 5 s. The tunnels have square cross section and the tip surface is smooth, although sometimes what appears to be growth facets are present, as on the right. There is a well-defined right angle edge between tip face and wall; no rounded contours are evident. Crystal structure not only determines the direction of tunnel growth, but the tunnels grow by crystallographic dissolution. In contrast to the flat, generally featureless tip surface, the walls are highly rippled with matching contours on adjacent walls. The wall-ripple density is the same at 90°C and 70°C: ~10^5 cm^{-1}.

It was thought that because of the active nature of the tunnel tip dissolution might occur for some interval that would alter the tip appearance after the external current was shut off.

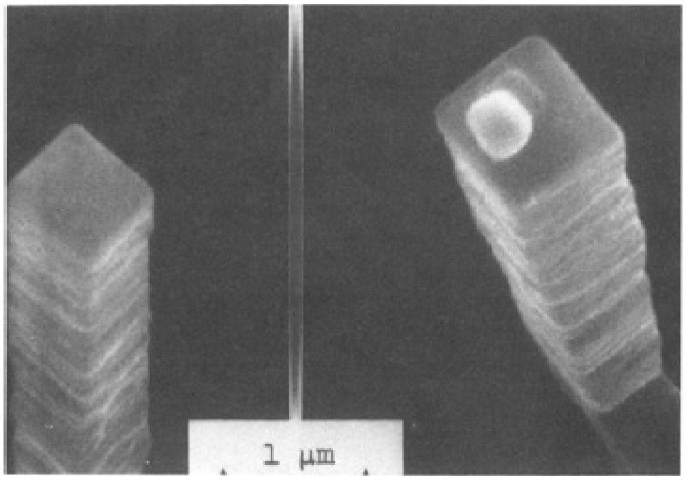

Fig. 2. Tunnel tips at 70°C, 200 mA/cm², 5 sec

Lower temperatures tend to produce wider tunnels. The widest tunnels observed in this paragraph were about 7 µm, in samples etched at 60°C and 65°C. No tunnels initiated if the temperature were below 60°C. However, tunnels would continue to grow at lower temperature after tunnels had started at a higher temperature. For example, after 5 s at 90°C the temperature was lowered to 40°C by rapid addition of cold etchant, and the etch was continued for 20 s. A tunnel that propagated during this period is shown in Fig. 3. The wider end section of the tunnel developed during the 40°C etch.

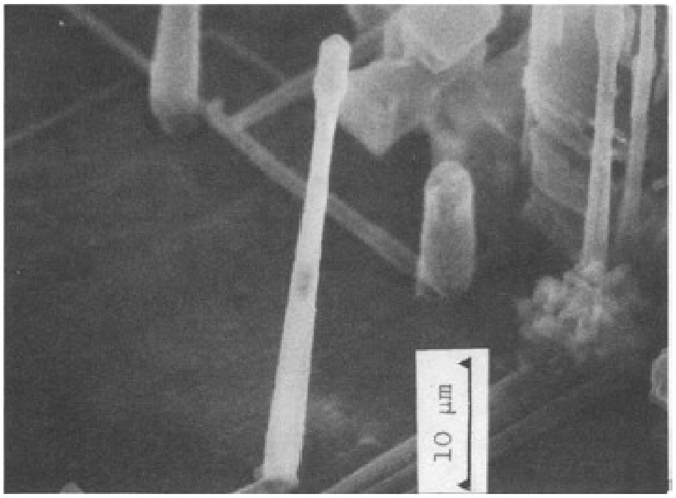

Fig. 3. Effect of temperature decrease from 90°C to 40°C during etch at 200 mA/cm^2. NaOH pretreatment.

Tunnel lengths were measured from micrographs like those in Fig. 1. Using the convention that the longest tunnels had initiated when the current was switched on, length *vs.* time was determined for these first generation tunnels. Different etch conditions were used and the several sets of data are plotted in Fig. 4. At longer times, the tunnel density is so high that the location of a tunnel base is obscured in 45° views. In those cases, the specimens were examined in cross sections prepared with conventional metallographic techniques.

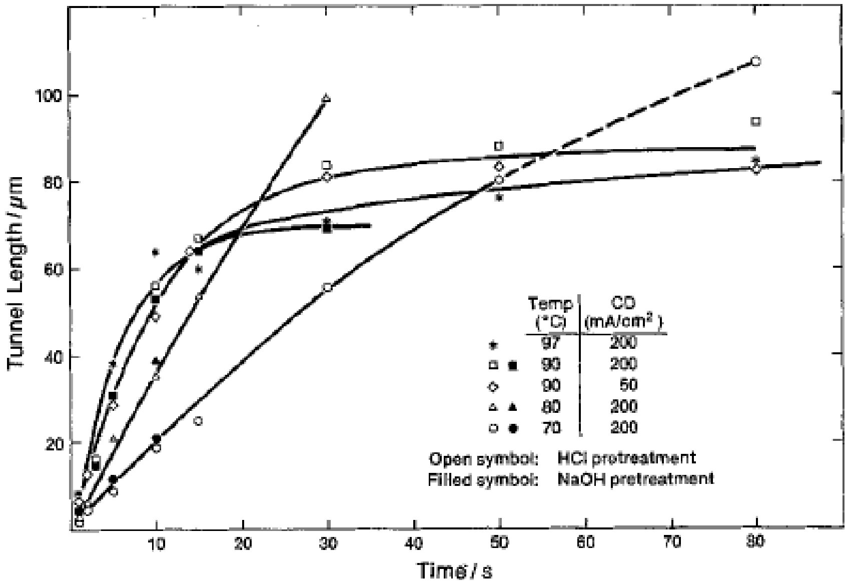

Fig. 4. First generation tunnel lengths. Open symbols for HCl pretreatment and filled symbols for NaOH pretreatment. ○: 70°C, 200 mA/cm^2; △: 80°C, 200 mA/cm^2; ◇: 90°C, 50 mA/cm^2; □: 90°C, 200 mA/cm^2; ✱ : 97°C, 200 mA/cm^2.

From Fig. 4, it is seen that neither pretreatment nor nominal c.d. had an effect on individual tunnel growth rate, although tunnel density and tunnel width depended on these particular conditions. Conditions that affect tunnel initiation do not necessarily have any effect on subsequent tunnel growth.

The initial tunnel growth rate increased with increasing temperature. At 70°C and 80°C the growth rate was constant up to ~55 μm length and decreased slightly at longer lengths. The dashed portion of the 70°C curve indicates that tunnels perforated the specimen at 80 s. Therefore, a longer tunnel length would have been recorded if a thicker foil had been used.

Tunnel growth at 90°C and 97°C was quite different than at the lower temperatures. Up to 65-70 μm, the length increased as $t^{0.7}$, and the growth stopped when tunnels reached a length of 70-90 μm.

Initial growth rate *vs.* 1/T is shown in Fig 5. An additional data point at 60°C (not shown in Fig. 4) is also included. An apparent activation energy of 15 kcal/mol describes the process over the whole temperature range.

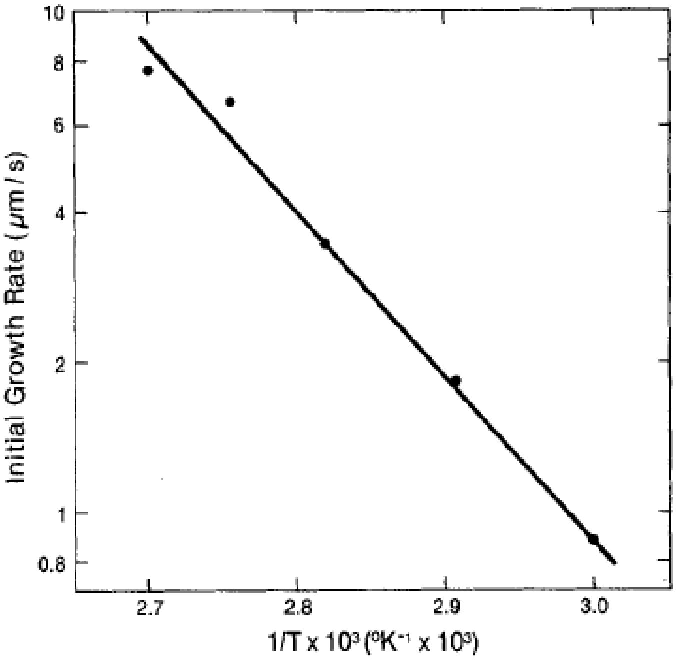

Fig. 5. Initial growth rate vs. reciprocal absolute temperature

2.2 Influence of low Temperatures [A16]

The mechanism for steady state tunnel growth is the same from 28 to 97°C. At temperatures of 60°C and below there is a transition period between crystallographic ½ cubic pit growth and steady state tunnel growth, in the range 1-10 s. The transition times decrease with increasing temperature, and are not found at 70°C or higher temperature. During this period, tunnels grow at high constant rate, about one-third the rate for pit growth, and the activation energy is the same as for pit growth. Tunnel appearance is different from steady state tunnels. There is no axial symmetry and no wall ripples. Instead, the tunnels have the appearance of stacked blocks, offset one from the other. It is suggested that this structure is the result of current interruptions and that transition tunnels lengthen by a process that can be likened to sequential pit growth. Dissolution occurs at the repassivation potential. Aluminum ions move from metal to solution through a chemisorbed Cl layer that is less stable than the layer present during steady state tunnel growth, but more kinetically accessible at these moderate temperatures.

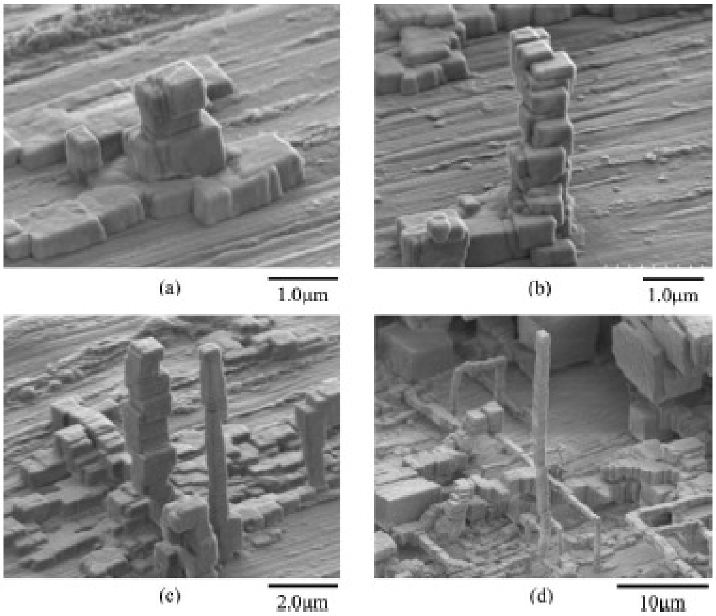

Figure 3. Tunnels grown at 28°C and 200 mA cm^{-2} for (a) 1, (b) 4, (c) 10, and (d) 200 s.

The length of the longest tunnel at each temperature is plotted *vs* etch time in Fig. 7a and b. Two regions are evident: initial fast tunnel growth for several seconds, followed by slower tunnel growth at longer etch times. Details of early tunnel growth are shown in Fig. 7b. The data for 50°C and lower temperatures show constant tunnel growth rates during this initial rapid tunnel growth period, referred to hereafter by the abbreviation, IRTG. The IRTG period gets shorter with increasing temperature, and at 60°C only the measurement at one second is within this region. The intercept of ~1 μm is due to the growth of hemispheric pits and ½ cubic pits when current is first applied. This precedes tunnel growth and occurs over a time scale much shorter than for tunnel growth. From
Fig. 7b we deduce that the short, irregular tunnels shown in Fig. 3 were produced during IRTG.

The transition from IRTG to steady state tunnel growth appears to be relatively abrupt, of the order of 1 s or less.

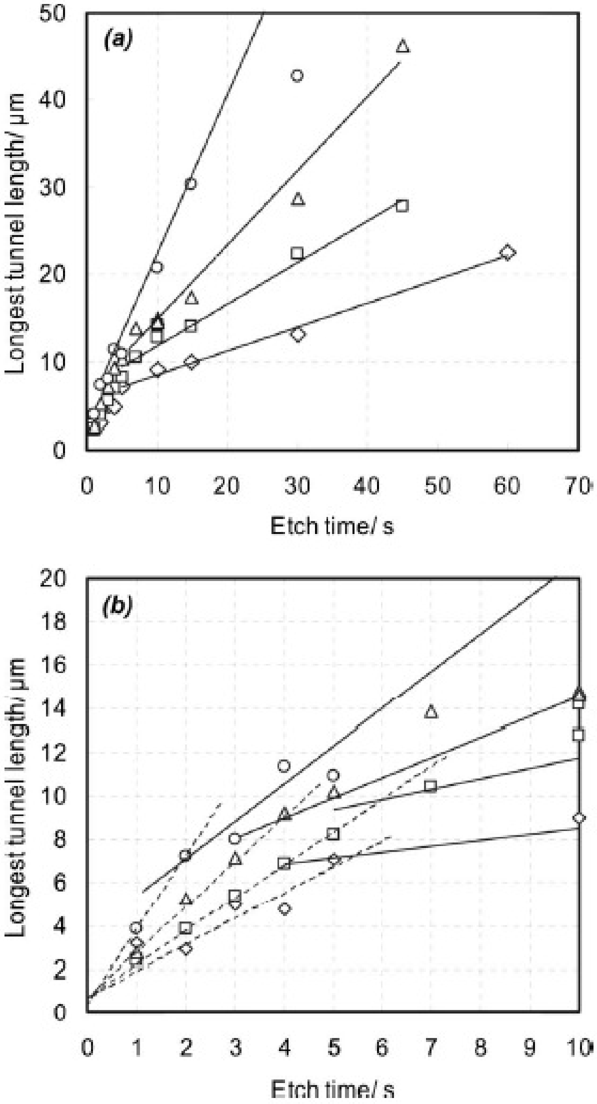

Figure 7. Longest tunnel length vs etch time. (a) 0–70 s etching time, (b) 0–10 s etching time. (◇) 28, (□) 40, (△) 50, and (○) 60°C.

3 - Transport resistance as limiting factor in tunnel growth [A5]

Under the hypothesis that the active surface at the tips of aluminium etch tunnels are continuously mantained at the repassivation potential of aluminium, Figure 7 shows that tunnels do not grow if the etchant is saturated with $AlCl_3$. This result, along with the decrease of dead tunnel geometry parameters with increasing concentration, indicates that: (i) tunnels stop growing when their tips become saturated in $AlCl_3$; (ii) the resistance to transport of $AlCl_3$ increases with increasing tunnel length.

If the transport resistance is determined (at least partly) by diffusion, it would increase with tunnel length as observed; therefore, an attempt was made to predict the limiting tunnel lengths in Fig. 7 and fig 8 with a model which assumed that mass transport in the tunnel is only by diffusion.

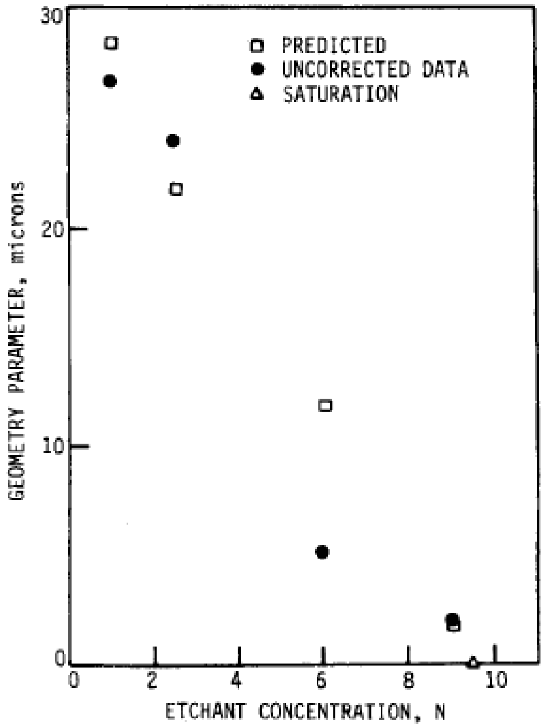

Fig. 7. Effect of aluminum chloride etchant concentration on geometry parameters of dead tunnels at 90°C.

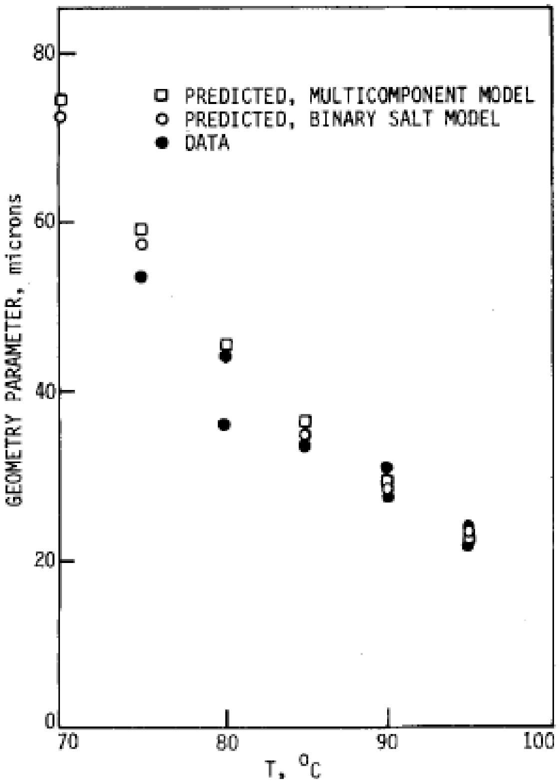

Fig. 8. Effect of temperature on geometry parameters of dead tunnels in 1*N* hydrochloric acid etchant.

The predicted ctitical geometry parameter if the tunnel electrolyte is an $AlCl_3$ binary salt is given by:

$P = w_1l/w_2 = (3\mathbf{F}/i)(C_{sat} - C_b)(D/t)_m$

where C is the electrolyte concentration (at saturation or bulk, mol/cm^3), D is the elctrolyte diffusivity (cm^2/s), “l” is the tunnel length (cm), “i” the current density (A/cm^2) and “w” the tunnel width (cm).

Hydrogen bubbles, if found within tunnels, would constitute an added transport resistance. It may be possible that hydrogen is evolved as part of the transition between

an active surface and a passive surface. This would not contradict the result that no obstructions are present during steady growth. Such a transition occurs in a current reduction experiment when a portion of the tunnel tip passivates.
One might envision the water of passivation as constituting a source of H_2

$Al + H_2O \rightarrow Al(OH) + 1/2\ H_2$

Hydrogen might also be formed during the growth of the oxide film to its steady thickness of several monolayers. In either case, the passivated surface would produce a finite amount of hydrogen gas which could wedge in the tip of the tunnel and obstruct mass transport.

4 – Spontaneous corrosion and pre-etching technique

The spontaneous attack of aluminum foil in a solution of $AlCl_3$, HCl acid, it is not easy to be realized, so we must use a technique that consists in an attack with electrochemical current impose (process in one step) or a two-step process, where the first phase consists of an attack with imposed current (pre-etching) and the second phase consists of a spontaneous attack, in the same solution used for activation.

In 1994 Giorgio Frassone [FR] performed a study of the spontaneous process of corrosion that provides the results described as follow.

The processes of activation, in those experiments were always performed at a current density of 0.105 A/cm^2 for etching times of 45 s, 90 s, 180 s, in solutions of 1% and 3% of free HCl. The process of spontaneous corrosion has been studied after a 90 s pre-etching for times of 120 s, 180 and 300 s.
Were analyzed: i) the loss in weight, ii) the number of tunnels, iii) the average diameter of the tunnel; iv) the average length of the tunnel; v) the specific capacity.

The experimental results obtained are then discussed.
In the process of pre-etching the spontaneous corrosion is always present and is mainly of generalized type, on the whole surface of the aluminum tape/foil.
In the case of spontaneous corrosion, the attack began with the pre-etching continues and there is a growing fact of the loss in weight. The surface not affected by the formation of tunnel works as a cathode area for the development of hydrogen, while the tunnels work ad anodic zones, both on the tunnels' walls and on the bottom. This fact is detected by the analysis of the growth of the diameters of the tunnels and theirs length, simultaneously. While the cathodic area remains virtually constant, the anodic area (which at the beginning of the spontaneous attack is 8-10 times the cathodic one) continues to increase for the increasing of diameters and length of the tunnels and, in experiments, reaches up

to 30-35 times the cathodic area. In the development of the size of the tunnels, the length tends to reach a threshold, about 30 μm, while the tunnels continue to increase in diameter. It was found that from 180 s to 300 s, the corrosion rate tends to decrease for the intervention of concentration polarization and for the change of pH in the tunnel.

5 - Initial events during the passivation of rapidly dissolving aluminium surfaces

The early stages of oxide film passivation of corroding surfaces in aluminum etch tunnels and pits were investigated [A9]. Passivation was initiated by step reductions in applied current. A mathematical model for passivation was used to predict experimentally measured potential transients during the first millisecond after the current step. The experimental transients had a characteristic potential undershoot at about 70 μs after the current step; according to the model, the undershoot was directly related to the partial coverage of the corroding surface with an oxide layer. The time and extent of the undershoot were in quantitative agreement with the theoretical predictions, suggesting that the fractional actively dissolving area in the pit at these times is a linear function of potential and adjusts rapidly to changes of the potential. This reconfiguration of the active area occurs at times when the extent of passive film formation is still small. A chemical mechanism for passivation which is consistent with the model is one in which the fractional active area is controlled by the coverage of specifically adsorbed chloride ions. Agreement between experimental and predicted potential transients was also observed at room temperature, where no tunnels are found, but only corrosion pits with irregular shapes.

Depassivation of corroding surfaces is attributed by various authors to factors such as solution acidity, or to salt films and adsorbed layers, the presence of which blocks access of passivating water to the metal.

In this chapter, a mathematical model was developed which describes the progress of passivation at times of less than 1 ms after its initiation. In particular, the model assumes that the surface being passivated is always heterogeneous, consisting of separated active and passive areas.

5.1 Experimental

Etching was carried out at 65°C in 1N HCl solution which was prepared from reagent grade HCl and deionized water. Prior to etching experiments, specimens were pretreated in 1N NaOH solution at room temperature for 20 min, washed with water, and dried in air. Samples etched after this pretreatment were found to contain a uniform tunnel length distribution, and also the extent of passivation was approximately uniform on each tunnel.

5.2 Potential transients

The applied current waveform, t_s, the time at which the current was stepped to a lower value, was usually 5 s. i_{a2}/i_{a1}, the ratio of the final to initial applied currents, was between 0 and 0.75. Potential transients are shown in Fig. 2, at times on the order of 1 ms after current step reductions. The potential decays rapidly to a minimum after the current step. The capacitive charging current, which is proportional to the time derivative of the potential, is zero at the potential minimum; at this time, the faradaic current has adjusted to the reduced applied current. Current cycling experiments, combined with weight loss measurements, showed that the reduction of faradaic current is achieved by a decrease of metal dissolution rate from tunnel tips and not by an increased rate of cathodic hydrogen evolution. Where i_{a2} is larger than zero, there is an abrupt potential increase after the potential minimum, which is followed by a slower relaxation to a steady potential.

The initial potential decay can be considered as two sequential potential decreases, ΔE_1 and ΔE_2, as shown in Fig. 3, in which the transient is depicted at much longer times than in Fig. 2. ΔE_1, the difference between the initial and final steady-state potentials, is a change of the ohmic potential drop in the bulk solution due to the decreased current flow to the counterelectrode. The remaining potential drop ΔE_2 is associated with individual pits or tunnels, and includes changes of the ohmic potential drop in the solution inside tunnels, as well as changes of the potential at the dissolving tunnel tip surface.

$$(\Delta E_2)_\Omega = (1 - i_{a2}/i_{a1})\,(i_{do}\, v\, t_s / \kappa) \qquad (5e1)$$

where i_{do} is the dissolution current density (A/cm^2), t_s is the difference between time of current step and time when current initially applied (s), “v” is the dissolution velocity (cm/s) and κ the solution coductivity inside tunnel (1/ Ω cm).

The main contribution to ΔE_2 is the variation of the potential at the surface being passivated.

Since the steady-state etching current is controlled by the ohmic resistance of the bulk solution, as the repassivation, or protection potential of the metal. Thus ΔE_2, when corrected for the ohmic contribution according to the equation above (5e1), can be identified as a surface overpotential relative to the repassivation potential.

It is clear that η_s, the surface overpotential (V) ,is the driving force for repassivation.

The active area is related to the potential by:

$$A/A0 = 1 + k\,\eta_S = 1 + k_{eff}\,(E-E_0) \qquad (5e2)$$

where k is an empirical constant relating fractional active area to potential (V^{-1}), k_{eff} is the modified k to account for ohmic resistance of tunnel (V^{-1}), E is measured potential corrected for bulk solution ohmic potential drop, E_0 is steady-state potential corrected for bulk solution ohmic potential drop, V; (also repassivation potential at bulk solution composition), and E_R is empirical repassivation potential of aluminum, (all in V).

5.3 Discussion of the mechanism of passivation

The active area is believed to be defined by the presence of a chloride containing surface layer whose coverage depends on potential.

The configuration of the surface layer is determined during the first tens of microseconds after the current step, when the surface is relatively free of oxide film. Chloride ions specifically adsorb on most of these surfaces; their coverage is in general zero near the potential of zero charge (E_{pzr} and increases monotonically as a function of potential (in many cases, approximately linearly) above E_{pzr}. On corroding aluminum surfaces, the potential of unit coverage would be the repassivation potential E_R, since at this potential surfaces in pits dissolve uniformly ($A/A_0 = 1$).

E_{pzr} of aluminum has not been measured directly, because the surface oxide film is always present when the metal is in contact with aqueous solutions. However, on the basis of the correlation between work functions and the potentials of zero charge, it has been estimated the E_{pzc} for aluminum at 25°C to be -0.84 V *vs.* the normal hydrogen electrode, or -1.03 V *vs.* the Ag/AgCl reference electrode. This correlation is obeyed for other metals to within 50 to 100 mV.

As the potential is decreased from the repassivation potential, E_R, to E_{pzc}, a range of 126 mV, the chloride surface coverage should decrease from unity to zero.

The present model suggests that reversible anion adsorption occurs only at very early times during passivation, when the oxide film has not yet fully formed. Once the oxide film is present, Eq. above (5e2) no longer determines the anion coverage: as the potential increased from its minimum value to E_R, the active area did not increase but remained constant.

6 - Kinetical effects

6.1 A model for the initiation of aluminium etch tunnels [A11]

In 1998 Zhou and Herbert presented the following simulation which predicts the spontaneous shape evolution of cubic etch pits on aluminum as they develop into etch tunnels during anodic etching in chloride solutions. The simulation is based on a model for oxide passivation, according to which the rate of oxide film coverage increases as the potential at the dissolving surface is made more negative than the critical repassivation potential, which depends on the local chloride ion concentration.

Mass transport calculations are used to predict the electrolyte concentration and potential in the pit, which in turn determine the rate of oxide advance and hence the shape change of the pit. The model predicts the pit-tunnel transformation, as well as width expansion of tunnels near their mouths. The occurrence of these features is independent of the choice of the passivation rate constant, an adjustable parameter in the simulation. Tunnel width oscillations were found at relatively low values of the rate constant. In the model, the pit-tunnel transformation is produced by rapid pit sidewall passivation, which is due to the relatively slower increase of the pit electrolyte concentration relative to the ohmic drop, during the pit's initial growth. A fully quantitative comparison of the model and experiment is possible with independent experimental information on passivation kinetics.

Characteristic features of tunnel morphology and growth have been discussed by Alwitt *et al.* [A2]. Tunnel growth occurs only in the <100> crystallographic directions. The growth velocity is independent of tunnel length but increases with temperature according to an Arrhenius dependence (activation energy 15 kcal/mol) The dissolving end or tip face is a flat and smooth (100) plane, while the sidewalls have a rough, corrugated texture (Fig. 1).

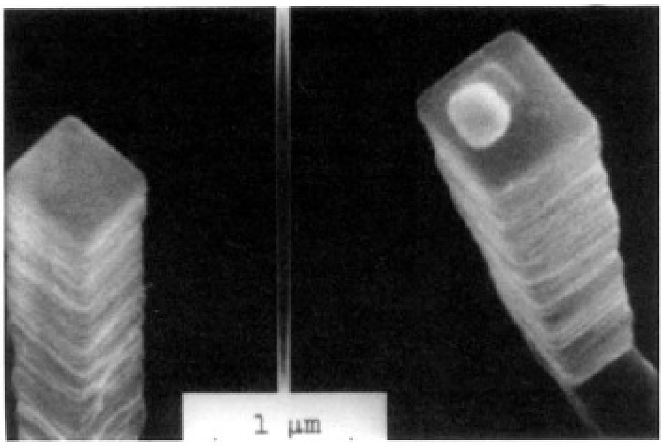

Fig. 1. Scanning electron micrograph of oxide replica of the etched aluminum surface showing the corrugated or rippled texture of tunnel sidewalls. Etching was carried out in 1 N HCl at 70°C at an applied current density of 0.200 A/cm^2. From Ref. 1, used by permission of the The Electrochemical Society (micrograph acquired by H. Uchi).

These wall ripples can be viewed as tunnel width oscillations, which have a characteristic amplitude and wavelength of roughly 0.1 µm; available information suggests that these ripple dimensions do not depend significantly on temperature. The widths of tunnels near their mouths expand with increasing length (Fig. 2), while those of long tunnels taper slowly. At small etching times (< 1 s), only half-cubic crystallographic etch pits, having (100) faces, are found on the surface, while after a few seconds, both etch pits and tunnels are present. This suggests that tunnels originate from etch pits, which transform into tunnels as they grow. After nucleation of etch pits, there is a stage of rapid dissolution in which they grow to sizes of 0.1—1 µm in a few milliseconds; afterward, their dissolution rate (or dissolution current density) is apparently constant and approximately the same as in tunnels. The dissolution rate in etch pits is uniform along their walls (Fig. 3).

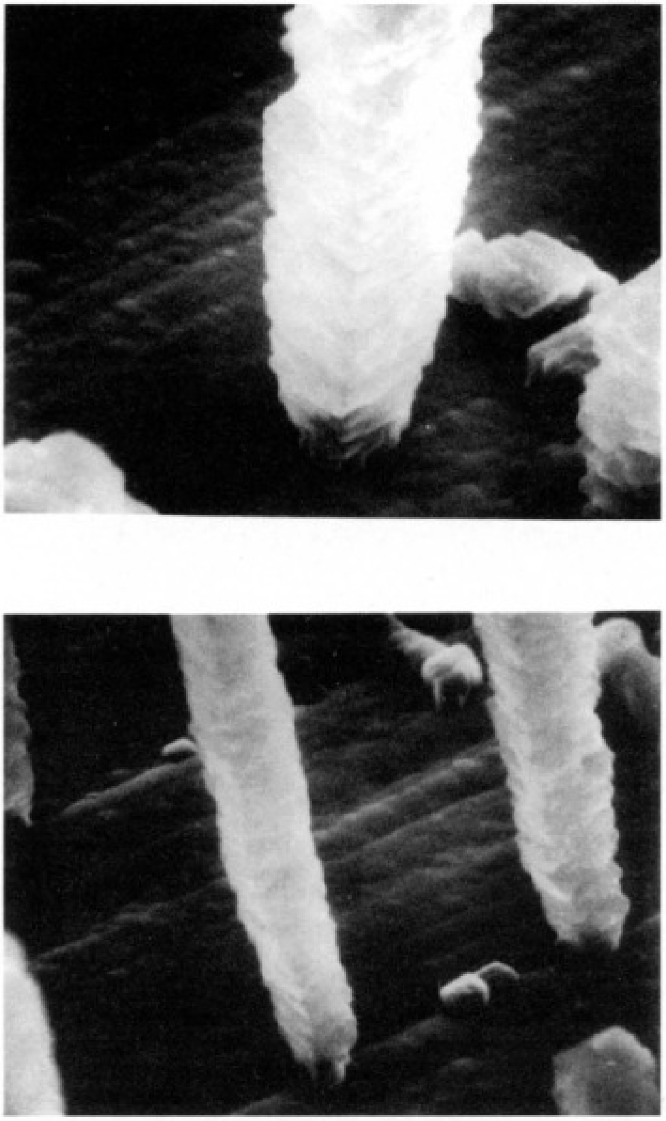

Fig. 2. Scanning electron micrograph of oxide replica of the etched aluminum surface showing width expansion of tunnels during their initial growth. Etching was in 1 N HCl at 0.200 A/cm^2 for 5 s. Etchant temperature (a) 70 and (b) 90°C. (Used by permission of R. S. Alwitt, micrograph acquired by H. Uchi).

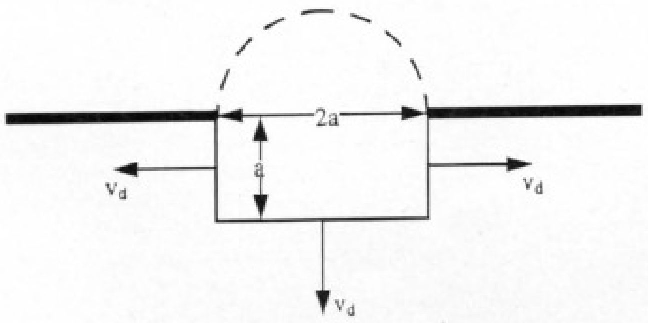

Fig. 3. Schematic depiction of the cross section of a half-cubic etch pit showing the location of the hemisphere used as the boundary in the simulation (dashed semicircle). The half-cubic shape represents the initial pit shape assumed in calculations. v_d is the dissolution velocity. The thick line represents the oxide film.

Aspects of the growth mechanism of tunnels can be inferred from their morphology. The passivity of tunnel sidewalls can be attributed to the presence of a surface oxide film. While the tunnel end surface dissolves, new oxide film is continuously formed on the sidewalls. The observation that the dissolving tip surfaces of tunnels are always flat and smooth suggests that this new oxide is formed only at the edge of the tip surface. In effect, the leading edge of the oxide film (oxide front) moves in the direction of tunnel growth, at a velocity (denoted here as v) which is the same as that of dissolution (v_d). In contrast to tunnels, the sidewalls of cubic pits are free of oxide film; the transformation of pits into tunnels is attributable to oxide passivation of the pit sidewalls. The characteristic width expansion of tunnels near their mouths suggests that this sidewall passivation does not occur instantaneously; rather, the oxide front moves down the sidewall with a finite velocity, while the exposed sidewall surface below the oxide front dissolves laterally (see Fig. 4a). Since the oxide front eventually reaches the dissolving pit bottom, v_p must be greater than v_d while the pit sidewalls are being passivated. However, after the oxide front arrives at the pit bottom, the two velocities are equal and remain equal during the further growth of the pit as a tunnel.

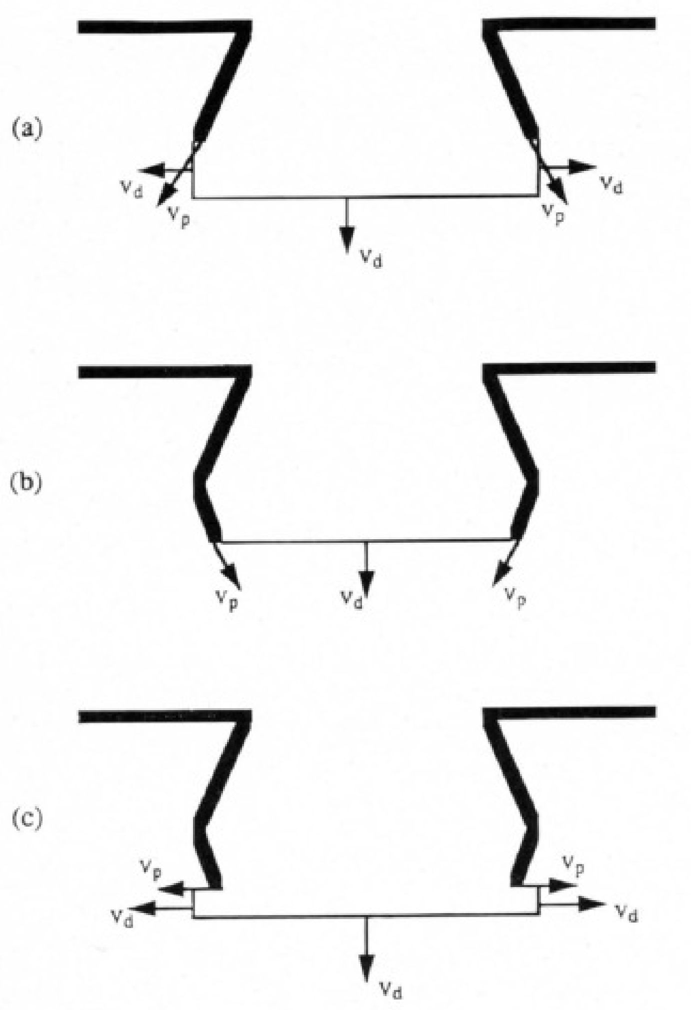

Fig. 4. Schematic depiction of three pit geometries for which different differential equations were applied to calculate the shape change of the pit. The thick line represents the oxide film. v_d is the dissolution velocity and v_p the velocity of the oxide front. (a) Gradually expanding width. (b) Gradually contracting width. (c) Discontinuously expanding width.

The model is based on two major concepts: (i) passivation takes the form of the movement of the leading edge of the oxide film into the pit along its sidewalls;
and (ii) the oxide front velocity is a function of the difference between the potential at the dissolving surface and the critical repassivation potential, whose value depends on the local chloride ion concentration. These concepts are derived from prior experiments and observations about the development of tunnel morphology. The simulation predicts the spontaneous pit-tunnel transformation and the width expansion of tunnels near their bases, as well as the presence of tunnel

width oscillations. It was found that the repassivation overpotential (difference between the potential and repassivation potential) needed to passivate the pit sidewalls during the transformation is generated by transient diffusion during pit growth, since the ohmic potential drop in the pit increases rapidly relative to the pit concentration overpotential. When the oxide front reaches the bottom surface of the pit, the rate of oxide advance slows an then oscillates around the metal dissolution rate as the pit continues to grow as an etch tunnel. The pit-tunnel tranformation is found to occur independently for the assumed value of the passivation rate constant, an unknown parameter. The passivation rates predicted by the model are somewhat smaller than those implied by the geometries of actual pits. This discrepance is thought to arise because the simulation does not allow passivation during the rapid initial growth of pits and does not include the effect of the moving boundary associated with the dissolving surface.

The concept that the passivation rate is a function of the diffeence between the potential and the repassivation potential differs from the other models of passivation, wich associate passivation with critical solution compositions or mass-tranfer rate.

6.2 Metal dissolution kinetics in etch tunnels

The potential dependence of the metal dissolution current density of aluminum in etch tunnels was measured, in year 2000 by Tak *et al.* [A12], using pulsed increases of current during galvanostatic etching experiments. Etching was carried out in 1 N HCl solution at 65°C, and was followed by analysis of the topographic development of the dissolving surfaces using scanning electron microscopy. By manipulation of the current waveform, the dissolving area and the applied current were varied independently. Parallel experiments with current interruptions were used to help identify the area of the dissolving surfaces during the anodic pulse, which were shown to be submicron size patches on the tunnel tip surfaces. After correction for solution-phase potential drops, the current was found to obey an exponential Tafel dependence on potential. Measurements of the dissolved depth *vs.* time show that the rate of cathodic hydrogen evolution is significantly increased during the anodic pulse, by comparison with that at the more negative potentials during constant current etching.

The purpose of the anodic current pulses is to stimulate increased metal dissolution in existing tunnels. However, to properly interpret the experiments, it is important to account for the effects of the anodic current pulses on other electrochemical processes as well, namely, the nucleation of new pits and oxidation on the filmed portion of the surface. For this purpose, two parallel sets of experiments were carried out, one in which the anodic pulses follow current interruptions, and the other where they follow pulsed current reductions. Figure 1 shows the general applied current waveform which describes both types of experiments, and defines the waveform parameters used in the later discussion. Values of these parameters are given in the figure captions for individual experiments. A period of 5 s at applied current density i_{a1} served to initiate tunnels and grow them to a length of about 10 μm. The anodic pulse is the period of duration t_H with applied current density i_{a3}. An intermediate period at lower current density i_{a2} immediately precedes the anodic pulse; in current interruption experiments, i_{a2} is zero, while in pulsed current reduction experiments, i_{a2} is between zero and i_{a1}.
During the current interruptions, the entire dissolving tunnel tip surfaces are covered with oxide film and thereby passivated. On the other hand, the current reductions from i_{a1} to i_{a2} cause only a fraction of the dissolving tip surface area to be covered with oxide, while the remainder continues to dissolve. Thus, anodic pulses after current interruptions will include only phenomena specific to oxidecovered surfaces, such as nucleation of new pits, oxide film growth, and metal dissolution through the oxide layer.

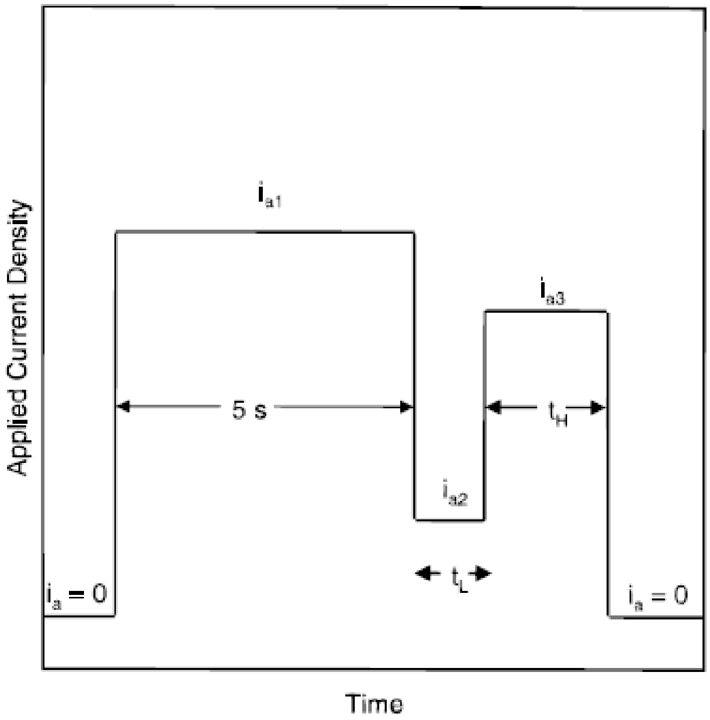

Figure 1. Schematic of applied current waveform, showing definitions of experimental variables. The anodic pulse is the period of length t_H when the applied current density is i_{a3}. i_{a2} is zero for the current interruption experiments, and between zero and i_{a1} for the pulsed current reduction experiments.

In experiments where the current was held constant for several seconds and then turned off, tunnel tip surfaces appear flat and featureless (Fig. 2a). The other micrographs in Fig. 2 show tunnel tip surfaces after experiments where anodic current pulses were applied after current interruptions. The anodic pulse time (t_H) in these experiments is 2 ms, and the interruption times (t_L) are 1, 8, and 40 ms. When t_L is 1 ms, the tip surfaces are fairly flat, but roughened by comparison with the case of no anodic current pulse. A large number of small pit-like features are found when t_L is 8 ms. However, when the interruptions are 40 ms or longer, the tip surface is again flat (Fig. 2d). The further development of tip surface morphology after current interruptions was investigated by increasing t_H to 20 ms (Fig. 3); here, i_{a3} is 10 mA/cm^2, and t_L is 4 ms in Fig. 3a, and 40 ms in Fig. 3b. As a result of continued metal dissolution during the longer anodic current pulse, distinct pits become apparent on the tip surfaces. These pits evidently grow from roughness features like those in Fig. 2c, suggesting that the surface roughness at t_H

of 2 ms is due to localized dissolution at a very early stage. The number of pits is significantly smaller when the interruption time is 40 ms, as opposed to 4 ms. When the interruption is 40 ms or longer, pits still form near the tunnel tip during the anodic pulse, but are as likely to be found on the sidewalls near the tip as on the tip itself. Pit formation during anodic current pulses after very short interruptions of a few milliseconds implies that an oxide film is present on the tip surface at the time of the anodic pulse.

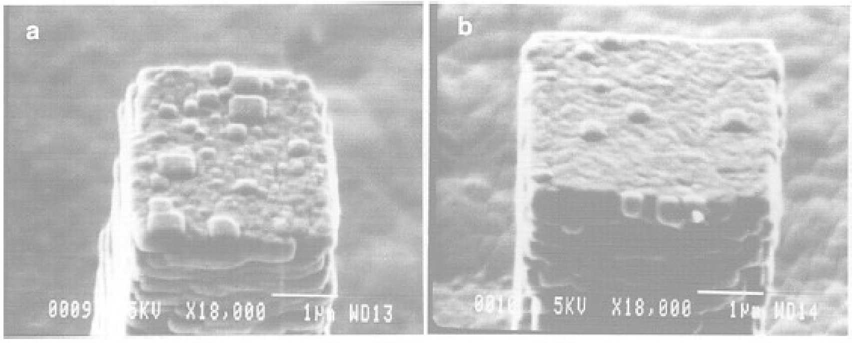

Figure 3. SEMs of replicas of tunnel tip surfaces after current interruption experiments, showing the effect of interruption time when the current pulse time t_H is 20 ms. i_{a2} is zero; i_{a1} and i_{a3} are 40 and 10 mA/cm^2, respectively. (a) t_L is 4 ms; (b) t_L is 40 ms.

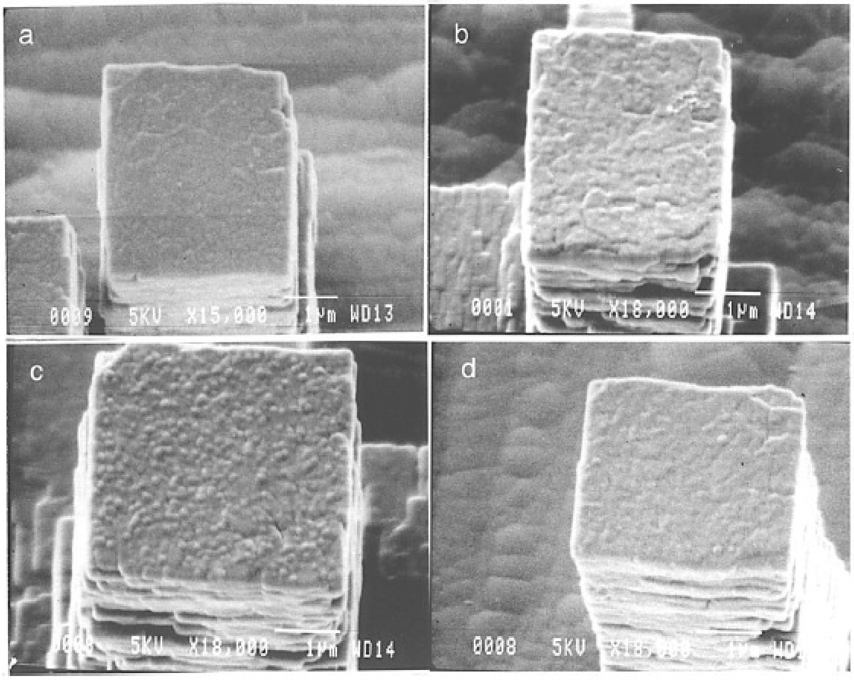

Figure 2. SEMs of replicas of tunnel tip surfaces after current interruption experiments, showing the effect of interruption time when the current pulse time t_H is 2 ms. (a) Current set to zero after 5 s at the applied current density (i_{a1}) of 40 mA/cm^2. For (b)-(d), t_H is 2 ms, i_{a2} is zero, and i_{a1} and i_{a3} are 40 mA/cm^2. (b) t_L is 1 ms; (c) t_L is 8 ms; (d) t_L is 40 ms.

Anodic current pulses were applied during anodic galvanostatic tunnel etching of aluminum, to investigate the kinetics of the metal dissolution reaction. The pulses, typically a few milliseconds in duration, were applied after a reduction of applied current for a period of a several milliseconds. When the reduced current prior to the anodic pulse is set to zero (current interruption experiments), the dissolving tunnel tip surface is passivated at the time of the interruption. The anodic pulse then produces nucleation of new pits on the tip and wall surfaces of tunnels, as well as dissolution and oxide growth on the passive surface.

In these experiments with the reduced current larger than zero, the current reduction causes the tip surface to partially passivate, leaving patches of dissolving surface surrounded by oxide film. During the subsequent anodic current pulses, the applied current is supplied primarily by enhanced metal dissolution from these patches. The kinetic relation between the dissolution current density and the potential (corrected for solution phase potential drops) was investigated; all these experiments produce a consistent dependence of patch current density on potential, which follows a Tafel equation for current densities up to 30 A/cm^2.

The rate of hydrogen evolution (the presumed cathodic process) is about five times larger during the anodic pulse compared to constant current etching.

6.3 Kinetic model for oxide film passivation in etch tunnels [A13]

The stability of localized corrosion cavities such as pits is determined by whether the dissolving surface inside the cavity can be passivated by formation of an oxide film. The process of oxide film formation is therefore of fundamental importance to all types of localized corrosion phenomena. Acidic pit solutions are necessary to prevent precipitation of oxide in the cavity solution. High concentrations of aggressive anions such as chloride are also considered to be important to maintain dissolution. Empirically, pits corrode freely only when the potential is more anodic than the critical repassivation potential, which is found to be a function of the aggressive anion concentration.

It is not known whether the film covers the dissolving surface as a front, or else forms as patches by two-dimensional nucleation, or by precipitation from the solution phase.

Passivation of the dissolving tip surfaces in tunnels can be induced in a controlled fashion by manipulation of the applied current during galvanostatic etching, and the progress of passivation then inferred from microscopic observations. Tak *et al.*, as seen in the previous paragraph, found that the initial effect of step reductions of applied current is to passivate portions of the interior of the tip surface, such that only small patches of dissolving area remain. At later times, all but one of these patches passivate. Hebert and Alkire [A11] modulated the applied current by sawtooth waves rather than by steps. They found that tunnel widths decrease continuously during the decreasing current ramp portion of these waveforms. Apparently, the ramps induce passivation only around the perimeter of the dissolving tip surface, rather than on its interior as in experiments with current steps.

Despite the highly concentrated solutions in tunnels, transport models can be readily constructed because the tunnel solution is approximately an $AlCl_3$ binary electrolyte, the tunnel geometry can be treated as one-dimensional, and transport is well approximated by steady-state diffusion and migration. [A11] Tak showed that the driving force for passivation is a surface overpotential, in this chapter denoted the “repassivation overpotential” η_R, defined as the difference between the potential at the dissolving surface and the empirical repassivation potential E_R. E_R depends on the chloride concentration at the dissolving surface according to

$$E_R = E_R^0 - B \log C_t \qquad [6e1]$$

In the current step experiments, η_R falls quickly to a minimum in a time of about 0.1 ms after the step, and then relaxes in a few hundred milliseconds to its initial value. Tak showed that the fraction of the tip area passivated increases linearly as the minimum ηR becomes more negative, and that the period when patches passivate one-by-one is the same as the η_R relaxation time. Further, the time of less than 1 ms in which passivation occurs is much smaller than the time needed for the diffusion to change the solution composition at the tip. This suggests that η_R is the fundamental variable controlling passivation, as opposed to factors related to solution composition alone, such as chloride concentration or pH.

Tak and Hebert suggested that η_R controls the adsorption of chloride ions on the dissolving surface whose presence shields the surface from passivating water molecules.

In the experiment conducted by Sinha and Herbert in the present chapter, current ramps rather than current steps are used to initiate passivation. Ramps produce passivation around the perimeter of the dissolving tunnel tip, as opposed to the step experiments in which oxide forms in the interior of the tip. Thus, ramps better simulate the type of passivation which occurs during the “natural” growth of tunnels at constant applied current. Ramp rates of 10, 20, 40, 60, and 100 mA/cm^2-s were used.

The current ramp causes the tunnel width to taper, as demonstrated by Fig. 1. The taper is due to the continuous encroachment of the dissolving tunnel tip surface by oxide film during the ramp time. The flat texture and orientation of the dissolving tip surface are unchanged by the ramp. This indicates that new oxide film does not form on the interior of the tip surface, but only along its edge.

Figure 1. Example of an SEM of an oxide replica of an etch tunnel after experiments with a decreasing current ramp. Ramp rate 10 mA/cm^2-s, ramp time 2 s, 5 s at constant current (40 mA/cm^2) before ramp.

The present work, coupled with that of Tak *et al.* described in the previuos paragraph, has provided a detailed picture of the dynamics of passivation in aluminum etch tunnels. In both current step and current ramp experiments, tunnel morphology studies have allowed the time-dependent geometry of oxide film coverage to be inferred. The rate of decrease of the active area is found to be composed of two additive contributions, one term proportional to the time derivative of the potential and the other term a Tafel-type rate expression in terms of the potential itself. Thus, the importance of the potential as the controlling variable for passivation is reinforced. Specifically, the potential driving force is the “repassivation overpotential”.

Critical acidification as a criterion for pit stability is not supported by the present results, although it may apply to pitting in solutions of higher pH for which oxide precipitation is possible. It is found here that passivation can be modeled most effectively in physical terms by desorption of chloride ions from an adsorbed layer on the dissolving surface.

7 - Two-step DC method [A17]

The distribution of initial etching sites in the acidic solution of HCl + H_2SO_4 is more uniform than that in the neutral solution of NaCl. But the acidic solution can corrupt aluminum foil; it will decrease aluminum foil's mechanical intensity. In order to obtain etched aluminum foil with higher density of tunnels and better mechanical intensity, a two-step DC etching is proposed in this chapter. Experiments indicated that the composition in the electrolyte during the second step DC etching process had great effect on the tunnel morphology.

Fig. 1 shows the SEM images of aluminum foil surface. The aluminum foil shown in Fig. 1a was etched in the solution of H_2SO_4 + HCl for 90 s at 75°C at 150 mA cm^{-1}, Fig. 1b and c shows the SEM images of aluminum foil etched by the two steps DC etching: the first step DC etching time was 90 s, the second step DC etching was 240 s, and the electrolyte during the second step DC etching process was the solution of NaCl with no addition or some organic compound respectively. The tunnels' size in Fig. 1a is smaller than that in Fig. 1b and c, tunnels' density in Fig. 1b is the most bulkiest.

Fig. 2 indicates that the number of tunnels with different size agrees with normal distribution basically. The average tunnels' size is 0.4 μm in Fig. 1a, and the tunnel density is 3.63×10^7 cm^{-2}. While the value are 0.75 μm and 3.72×10^7 cm^{-2}, respectively in Fig. 1b, the value are 0.80 μm and 3.43×10^7 cm^{-2} respectively in Fig. 1c. Those data showed that some new tunnels were fabricated at the second step DC etching when electrolyte was the solution of NaCl, the average size of tunnels etched at the first step DC etching process was enlarged from 0.4 μm to 0.75 μm in the solution of NaCl. However, there was no new tunnel to be fabricated at the stage of the second step DC etching when the solution of NaCl with addition of some organic compound was used as electrolyte during the second step DC etching process, but the average size of tunnels etched at the first step DC etching was enlarged at this stage.

Fig. 3 shows cross-section images of aluminum foil. Fig. 3a shows that the tunnels' length is about 24 μm when aluminum foil was etched in acidic solution for 90 s;

Fig. 3b shows that the value has no obvious change after the etched aluminum foil was etched in the solution of NaCl for 240 s. But the tunnels' length increases to 37 μm after the etched aluminum foil was etched in the solution of NaCl with addition of some organic compound for 240 s.

In Fig. 4a there are many branch tunnels, and it is vertical between main tunnels and branch tunnels. But few branch tunnel can be found in Fig. 4b and c. This means that branch tunnels can be fabricated by use of the two-step DC etching method proposed
in this chapter.

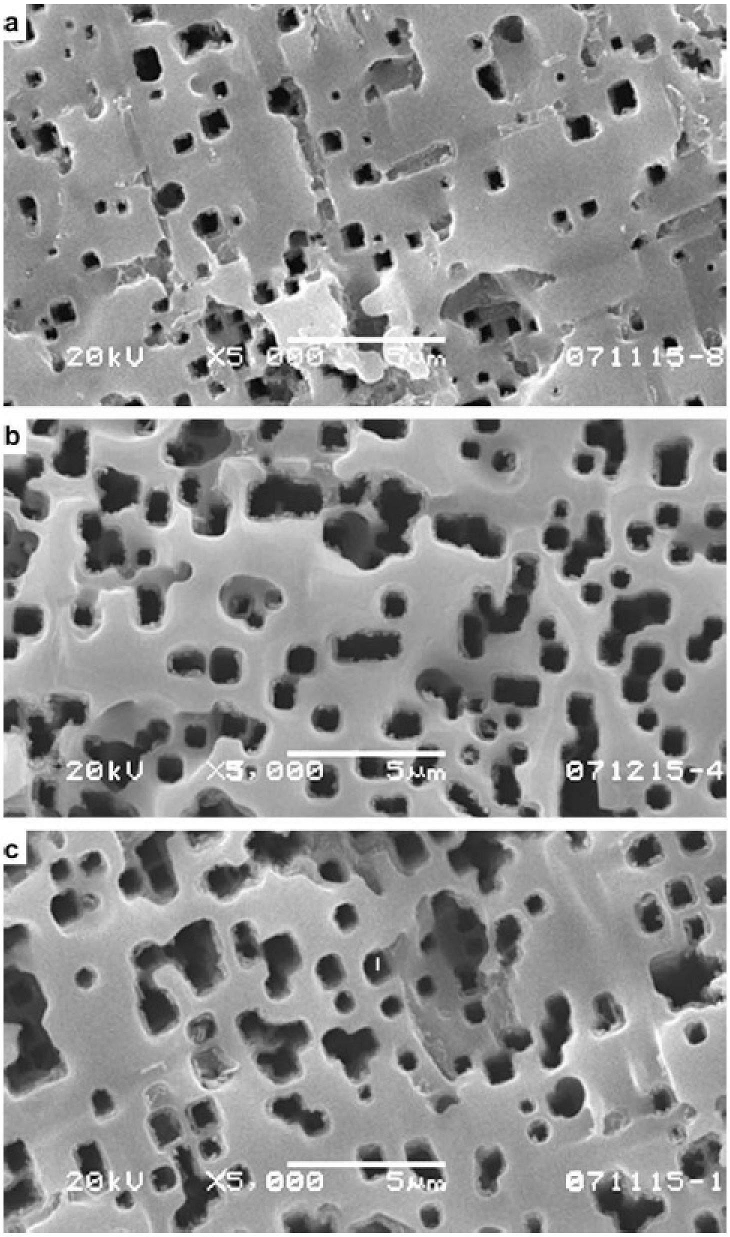

Fig. 1. SEM images of aluminum foil surface after anodic etching: (a) in an acidic solution for 90 s, (b) in an acidic solution for 90 s and then etching in a neutral solution for 240 s, and (c) in an acidic solution for 90 s and then etching in a neutral solution with addition of some organic compound for 240 s.

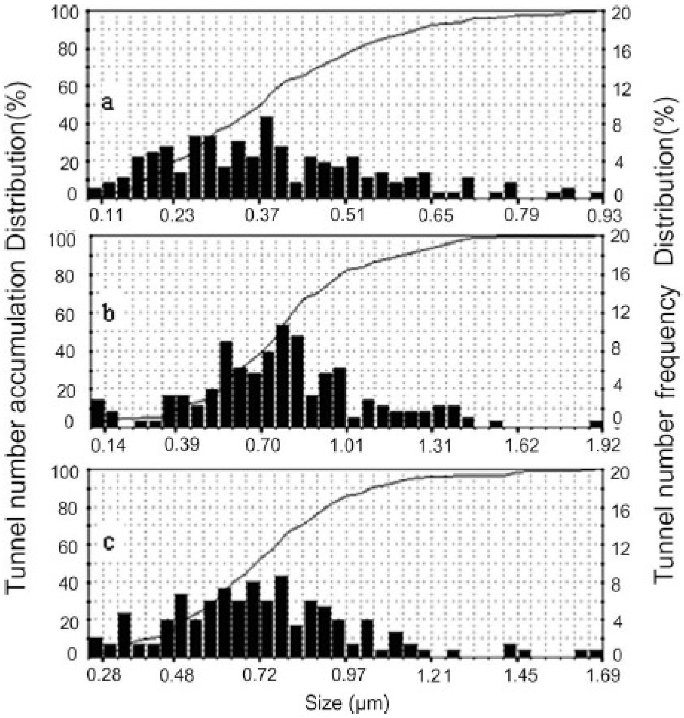

Fig. 2. Tunnel number accumulation distribution and tunnel number frequency distribution of aluminum foil surface after etching (a) in an acidic solution for 90 s, (b) in an acidic solution for 90 s and then etching in a neutral solution for 240 s, and (c) in an acidic solution for 90 s and then etching in a neutral solution with addition of some organic compound for 240 s.

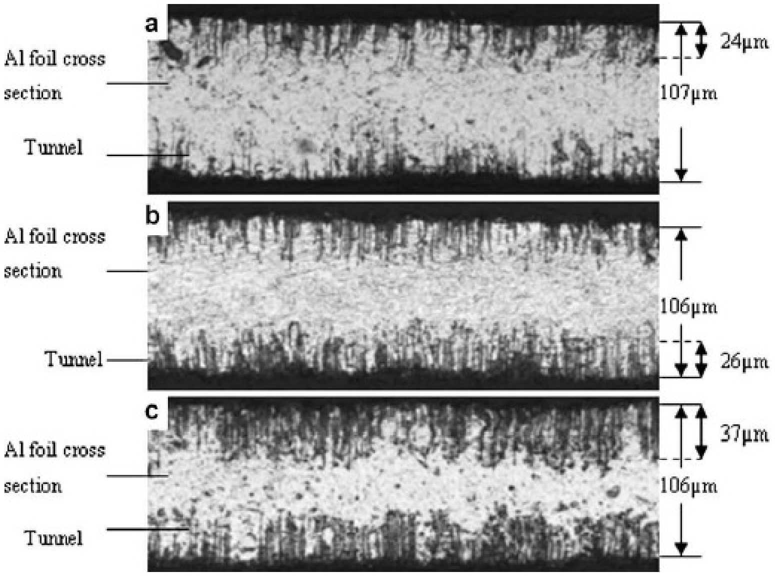

Fig. 3. Cross-section images of aluminum foil after etching (a) in an acidic solution for 90 s, (b) in an acidic solution for 90 s and then etching in a neutral solution for 240 s, and (c) in an acidic solution for 90 s and then etching in a neutral solution with addition of an organic compound for 240 s.

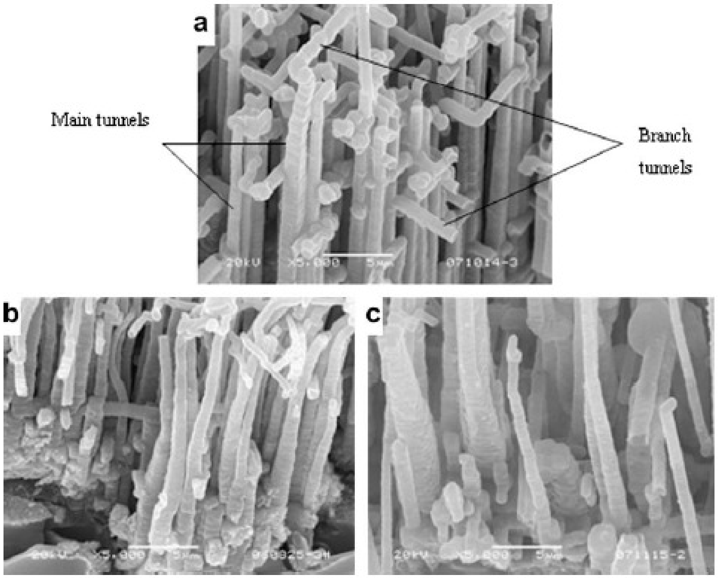

Fig. 4. SEM images of TiO_2 replicas of the tunnels' structure in aluminum foil after etching (a) in an acidic solution for 90 s and then etching in a neutral solution with addition of an organic compound for 240 s, (b) in an acidic solution for 90 s, and (c)in a neutral solution for 90 s.

According to Figs. 1 and 3, the composition of electrolyte during the second step DC etching has great effect on the tunnel morphology of aluminum foil after etching by use of the two-step DC etching. When the solution of NaCl is used as the electrolyte, the density and size of tunnels are enlarged, but tunnels' length has no obvious change.

After aluminum foil has been etched in acidic solution, the surface of aluminum foil changed to be more roughness via tunnels, so the pitting potential was decreased during the second step DC etching process.

Fig. 5 illustrates that there are many large holes on the surface of aluminum foil when the first step DC etching time is 30 s or 60 s. The pitting potential was higher at the second step DC etching process when the first step DC etching time was 30 s or 60 s, so the new tunnels produced at sites where it was easier for them to produce, such as impurity points. Therefore the new tunnels congregated with those tunnels etched at the first step DC etching process, and then many large holes on the surface of aluminum foil were formed. But the surface of aluminum foil changes to be smooth when the first step DC etching time is 90 s or 120 s in Fig. 5. Tunnels have dispersed equably on aluminum foil surface after the aluminum foil has been etched in acidic solution for 90 s, the effect of surface roughness on pitting potential was uniform at per place of aluminum foil surface, so the new tunnels produced equably on the aluminum foil surface, and then the surface of aluminum foil was smooth.

Fig. 4a shows there are many branch tunnels when some organic compound was dissolved in electrolyte during the second step DC etching process, and it is vertical between main tunnels and branch tunnels.

The organic compound was a key factor for the branch tunnels. The aluminum foil surface was covered with organic compound and new tunnel couldn't be fabricated during the second step DC etching. But the molecule of organic compound could not enter into tunnels' inner, so new tunnels would be fabricated on the side walls and tips of tunnels produced at the first step DC etching process. The branch tunnels can increase surface area of aluminum foil.

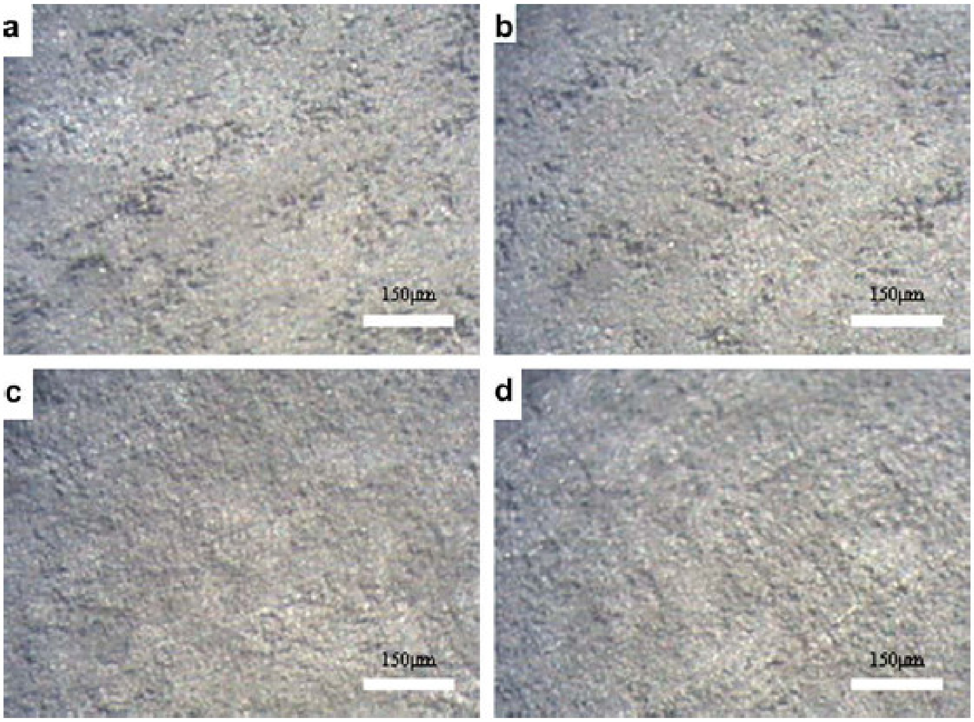

Fig. 5. Effect of the first step etching time on the surface morphology of aluminum during two-step DC etching (a: 30 s, b: 60 s, c: 90 s, d: 120 s).

8 – Conclusions

A high density of microscopic tunnels with high aspect ratio is produced by anodic etching of Al in a hot chloride-containing solution. This technology is widely used to make foil electrodes for Al electrolytic capacitors with high surface area.

- Etching at a temperature in the range 70–95°C creates tunnels ~1 μm wide and up to ~40 μm long, and these are randomly distributed at a density as high as 10^8 cm^{-2}.
- Tunnels grow in a <100> direction and the dissolving tip is a square (100) surface. The annealed Al foil used for electrolytic capacitors has more than 90% of the surface with (100) orientation, and therefore the tunnels grow perpendicularly to the surface.
- A tunnel is the end product of the sequence: hemispheric pit → ½ cubic pit → tunnel.
- The tunnel shape develops when the pit sidewalls passivate but the bottom pit face continues to dissolve. A tunnel lengthens because dissolution occurs only at the tip and the sidewalls passivate as the dissolving tip surface advances, leading to symmetric tunnel shape with high aspect ratio.
- The time for tunnels to initiate decreases as temperature increases. At 70°C tunnels are first seen at about 250 ms. Steady state tunnel growth occurs at constant rate with activation energy of 15 kcal/mol, from 97°C down to 50°C.
- The potential at the dissolving surface E_{tip} is the repassivation potential E_R. This potential is maintained because dissolution and passivation occur in parallel and E_R is the only potential at which both processes can occur. The repassivation potential at the tunnel tip is the same as E_R in an $AlCl_3$ solution of the same chloride concentration as at the tip.

In both current step and current ramp experiments, tunnel morphology studies have allowed the time-dependent geometry of oxide film coverage to be inferred.

- The rate of decrease of the active area is found to be composed of two additive contributions, one term proportional to the time derivative of the potential and the other term a Tafel-type rate expression in terms of the potential itself.

- The importance of the potential as the controlling variable for passivation is reinforced. Specifically, the potential driving force is the "repassivation overpotential".

A two-step DC etching method was proposed. Experiments indicated that the composition of electrolyte during the second step DC etching had great effect on the tunnel morphology of aluminum foil.

- When the solution of NaCl was used as the electrolyte, many new tunnels produced during the second step DC etching, the size of tunnels was enlarged; tunnels' length had no obvious change.
- The tunnels' length increased from 24 μm to 37 μm after the etched aluminum foil had been etched in the solution of NaCl with addition of some organic compound for 240 s, and many branch tunnels were fabricated on the side walls and tips of tunnels.

APPENDIX

Miller Index [W1]

Miller indices are a notation system in crystallography for planes and directions in crystal (Bravais) lattices.

In particular, a family of lattice planes is determined by three integers “l”, “m”, and “n”, the Miller indices. They are written (l,m,n) and denote planes orthogonal to a direction (l,m,n) in the basis of the reciprocal lattice vectors. By convention, negative integers are written with a bar, as in $\underline{3}$ for -3. The integers are usually written in lowest terms, *i.e.* their greatest common divisor should be 1.

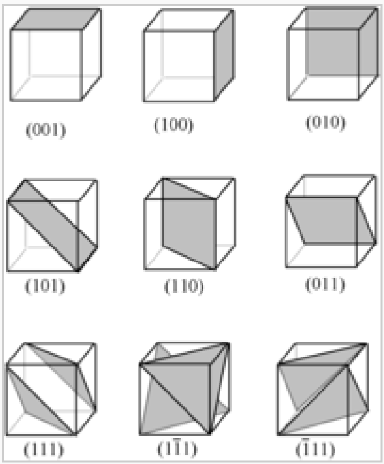

Planes with different Miller indices in cubic crystals

There are also several related notations:

- [l,m,n], with square instead of round brackets, denotes a direction in the basis of the direct lattice vectors instead of the reciprocal lattice;
- the notation {l,m,n} denotes all planes that are equivalent to (l,m,n) by the symmetry of the lattice;

- similarly, the notation <l,m,n> denotes all directions that are equivalent to [l,m,n] by symmetry.

REFERENCES

References in english

[A1] L. van Alpen, P. Nauwen, J. Slakhorst, *Z. Metallkde*, Bd. 70, 1979

[A2] R. S. Alwitt, H. Uchi, T. R. Beck, R. C. Alkire, *J. Electrochem. Soc.* – Vol.131, n.1, Jan 1984

[A3] T. R. Beck, *Electrochimica Acta* – Vol.30, n.6, 1985

[A4] K. Arai, T. Suzuki, T. Atsumi, *J. Electrochem. Soc.* – Vol.132, n.7, Jul 1985

[A5] K. Herbert, R. Alkire, *J. Electrochem. Soc.* – Vol.135, n.9, Sep 1988

[A6] R. M. Stevanovic, A. R. Despic, D. M. Drazic, *Electrochimica Acta* – Vol.33, n.3, 1988

[A7] T. R. Beck, *Electrochimica Acta* – Vol.35, n.10, 1988

[A8] B. J. Wiersma, K. R. Herbert, *J. Electrochem. Soc.* – Vol.138, n.1, Jan 1991

[A9] Y. Tak, K. R. Herbert, *J. Electrochem. Soc.* – Vol.141, n.6, Jun 1994

[A10] D. Good, *J. Electrochem. Soc.* – Vol.144, n.6, Jun 1997

[A11] Y. Zhou, K. R. Herbert, *J. Electrochem. Soc.* – Vol.145, n.9, Sep 1998

[A12] Y. Tak, N. Sinha, K. R. Herbert, Metal Dissolution Kinetics in Aluminum Etch Tunnels, *J. Electrochem. Soc.* – Vol.147, n.11, 2000

[A13] N. Sinha, K. R. Herbert, Kinetic Model for Oxide Film Passivation in Aluminum Etch Tunnels, *J. Electrochem. Soc.* – Vol.147, n.11, 2000

[A14] N. Osawa, K. Fukoka, *Corrosion Science* – 42, 2000

[A15] D. Park, H. Kim, *Analytical Science*, Vol.17 supplement, 2001

[A16] T. Makino, R. S. Alwitt, S. Ono, *J. Electrochem. Soc.* – Vol.154, n.2, 2007

[A17] R. Xiao, K. Yan, Tunnel morphology of aluminium foil etched by a two-step DC etching method, *Corrosion Science* – 50, 2008

[A18] R. Xiao, K. Yan, J. Yan, J. Wang, Electrochemical etching model in aluminum foil for capacitor, *Corros. Science* – 50, 2008

[E1] Jong-ho Ryu, Jong hyun Seo, Jae-han Jeong, Sung-kap Kim, Dong nyung Lee, *J. Appl. Electrochem*. 34 (2004) 883.

[E2] W. Lin, G.C. Tu, C.F. Lin, Y.M. Peng, *Corros. Sci*. 38 (6) (1996) 889.

[E3] W. Lin, G.C. Tu, C.F. Lin, Y.M. Peng, *Corros. Sci*. 39 (9) (1997) 1531.

[E4] Kamal Muthukrishnan, Kurt R. Hebert, Takeshi Makino, Interfacial void model for corrosion pit initiation on aluminum, *J. Electrochem. Soc*. 151 (6) (2004) B340–B346.

[E5] S. Ono, T. Makino, R.S. Alwitt, Crystallographic pit growth on aluminum(100), *J. Electrochem. Soc*. 152 (2) (2005) B39–B44.

[E6] E. McCafferty, *Corros. Sci*. 37 (3) (1995) 481–491.

[E7] A. Ben Rais, J.C. Sohm, Aluminum pit propagation in acidic media-II theoretical model, *Corros. Sci*. 25 (11) (1985) 1047–1056.
[E8] Jae-Han Jeong, A model for the (100) crystallographic tunnel etching of aluminum, *Journal of Materials Science* 31 (1996) 5811–5815.
[E9] Marta Verhoff, Richard Alkire, Experimental and modeling studies of single corrosion pits on pure aluminum in pH 11 NaCl solutions - I Laser initiated single pits, *J. Electrochem. Soc*. 147 (4) (2000) 1349–1358.
[E10] Marta Verhoff, Richard Alkire, Experimental and modeling studies of single corrosion pits on pure aluminum in PH 11 NaCl solutions - II Pits stability, *J.Electrochem. Soc*. 147 (4) (2000) 1359–1365.

[W1] http://en.wikipedia.org/wiki/Miller_index

References in italian

[FR] Giorgio FRASSONE, Incisione di nastro di alluminio per condensatori elettrolitici, *Tesi di Laurea in Ingegneria Chimica*, Politecnico di Milano, 1992-1993

Acknowledgments

*I really thanks the *M*aster and all of the people who trusted in him…*